

Feedback Beamforming in the Time Domain

Zvi Aharon Herscovici

Feedback Beamforming in the Time Domain

Research Thesis

Submitted in partial fulfillment of the requirements
for the degree of Master of Science in Electrical Engineering

Zvi Aharon Herscovici

Submitted to the Senate
of the Technion — Israel Institute of Technology
Tevet 5786 Haifa January 2026

This research was carried out under the supervision of Prof. Israel Cohen, in the Faculty of Electrical and Computer Engineering.

Some results in this thesis have been published as an article by the author during the course of the author's master research period, the most up-to-date versions of which being:

Z. A. Herscovici and I. Cohen, "Feedback beamforming in the time domain," <i>Sensors</i> , vol. 24, no. 7, p. 2179, 2024.

The author of this thesis states that the research, including the collection, processing and presentation of data, addressing and comparing to previous research, etc., was done entirely in an honest way, as expected from scientific research that is conducted according to the ethical standards of the academic world. Also, reporting the research and its results in this thesis was done in an honest and complete manner, according to the same standards.

Acknowledgements

First of all, I would like to deeply thank my research supervisor, Prof. Israel Cohen, for his invaluable guidance and critical insights. His support made this work possible. I am truly appreciative of the opportunities he provided and the trust he placed in me along the way.

I would also like to thank my family, my parents and my sisters, and to my partner, Lior, who fostered a supportive and inclusive environment, empowering me to perform my work with greater confidence and effectiveness. I am truly indebted to them, as this achievement could not have been realized without their contribution.

The generous financial help of the Technion is gratefully acknowledged.

Contents

List of Figures

Abstract	1
Abbreviations	3
Notations	5
1 Introduction	7
1.1 Background and Motivation	7
1.2 Overview of the Thesis	9
1.3 Main Contributions	10
1.4 Thesis Organization	10
2 Preliminaries	11
2.1 Shannon’s Sampling Theorem	11
2.2 Sensor Arrays	12
2.3 Beamforming	12
2.4 Temporal Digital Filtering Analogy to Spatial Signal Processing	13
2.5 Propagating Wave Fields	15
2.6 Array Performance in the Spatial Domain	17
2.6.1 Beampattern	17
2.6.2 The Normalized Beampattern	18
2.6.3 Peak-to-Sidelobe Ratio	18
2.6.4 Directivity	19
3 Time-Domain Feedback Beamforming: Model and Design	21
3.1 Problem, Signal Model and Notations	21
3.1.1 Feedback Beamforming	24
3.2 Fisher Information Matrix	27
3.3 Beamformer Evaluation	28
3.3.1 Channel Gain Estimation Error	29
3.3.2 Mainlobe and Sidelobe Attenuation	29

3.3.3	Directivity Factor	30
3.3.4	Range Error Influence	31
3.3.5	Summary	32
3.4	Time-Domain vs. Frequency-Domain Feedback Beamforming	33
3.4.1	Calculation Complexity	33
3.4.2	Execution Time	34
3.4.3	Summary	36
4	Conclusions	37
4.1	Future Research	37
4.1.1	Noisy Environment	38
4.1.2	Moving Target in Dynamic Environment	38
4.1.3	Multi Target	39
4.1.4	Adaptive Feedback Beamforming	39
A	Fisher Information Matrix	41
A.0.1	Cramér–Rao Lower Bound	41
A.0.2	Multiple-Parameter Case	42
A.0.3	Applications of the FIM	42
B	FIM Calculation	43
	Bibliography	45
	Hebrew Abstract	i

List of Figures

2.1	A ULA of N elements and inter-element spacing of δ	13
2.2	An FIR filter applied to signal x with coefficients k , generating a filtered signal y	14
2.3	IIR filtering of the input signal x using feedforward coefficients k and a recursive component defined by coefficient r , producing the output signal y	15
2.4	Two widely used methods are employed to visualize the 2D planar beam-pattern. Both plots illustrate the responses of 8-element and 16-element conventional beamformers, shown in blue and orange, respectively. On the left, the response is displayed over the $[0, \pi]$ angular range in decibels (dB). On the right, a polar plot presents the same response in dB, with the DOA expressed in degrees.	18
3.1	A spatial reference system illustrating the relationship between Cartesian and spherical coordinates in two dimensions.	22
3.2	Proposed beamformer structure. The goal is to spatially localize the target, P_t , by retransmitting the signal.	26
3.3	Feedback beamformer beampattern for different channel gain estimation errors for $\theta_d = 90^\circ$, $N = 10$ and $\delta = 1cm$	29
3.4	Feedback beamformer beampattern (blue line), compared to known ULA beamformers, DS (dashed red line), and maximum DF (dashed green line) respectively for $\theta_d = 90^\circ$, $r = 0.6$, $N = 10$ and $\delta = 1cm$	30
3.5	Directivity factor as a function of δ for the feedback beamformer (3.26) (lines with circles) compared to DF for a generic ULA (solid lines) for a signal wave with a frequency carrier of 1 GHz, $r = 0.6$, $\theta_d = 45^\circ$. DF was tested for several values of N : $N = 10$ (blue lines), $N = 20$ (red lines), $N = 30$ (green lines), and $N = 40$ (light blue lines).	31
3.6	Effect of incorrect target range estimation for $\theta_d = 90^\circ$, $r = 0.6$, $N = 10$ and $\delta = 1cm$	32
3.7	Power spectrum of both the pulse wave (blue line) and sine wave (red line) at the same sampling frequency.	35

3.8 Execution time of the beamformer output for both time and frequency domains for $r = 0.6$, $\delta = 1cm$, when 10K frequencies are considered. . . 36

Abstract

Spatial array processing constitutes a central framework in signal processing for source localization, interference mitigation, and spatial filtering. By exploiting the spatial diversity of sensor arrays, array processing methods enable the estimation of source parameters such as direction of arrival and range. Among these techniques, beamforming provides a structured mechanism for spatial selectivity by shaping the array response toward desired regions while suppressing undesired components. Classical beamforming approaches—including delay-and-sum (DS) and minimum variance distortionless response (MVDR) designs—are implemented as spatial finite impulse response (FIR) systems, whose achievable resolution and estimation accuracy are fundamentally constrained by the physical aperture and geometry of the array. Performance improvements within such feedforward architectures are therefore inherently bounded by aperture size, motivating the investigation of alternative structural paradigms.

Feedback beamforming addresses this limitation by introducing spatial recursion into the array processing chain, yielding spatial infinite impulse response (IIR) behavior that effectively extends the virtual aperture of the array without increasing the number of sensors. Unlike frequency-domain recursive formulations, the proposed architecture is implemented directly in the time domain, enabling causal and computationally efficient processing suitable for real-time applications. Prior studies have demonstrated that spatial recursion may enhance angular selectivity; however, performance has predominantly been assessed using beam pattern characteristics or signal-to-noise ratio (SNR) metrics. A systematic estimation-theoretic interpretation of time-domain feedback beamforming, particularly in relation to parameter identifiability and fundamental performance bounds, remains limited in the existing literature.

This thesis develops a coherent estimation-theoretic framework for time-domain feedback beamforming operating in a far-field region of interest, where direction and range parameters are jointly estimated. The analysis establishes explicit connections between spatial recursion, effective aperture extension, and achievable estimation accuracy in real-time processing settings. Parameter sensitivity is characterized using the Fisher Information Matrix (FIM), enabling direct assessment of the associated Cramér–Rao Lower Bounds (CRLBs) for the jointly estimated parameters. The analysis reveals that as the feedback gain approaches its optimal value, the denominator of the spatial transfer function approaches zero, amplifying the array’s spatial response and yield-

ing improved parameter sensitivity, providing a quantitative and estimation-theoretic formalization of virtual aperture extension. The comprehensive time-domain analysis presented herein is intended to serve as a theoretical ground base for future implementations of feedback beamforming in practical RADAR systems, including pulsed target detection, range estimation, and real-time spatial filtering applications.

The proposed architecture is evaluated using conventional beamforming performance metrics—beamwidth, peak-to-sidelobe ratio, and array directivity—demonstrating significant improvements over conventional delay-and-sum and maximum directivity beamformers across all measures. Furthermore, a comparative analysis between time-domain and frequency-domain implementations reveals that the time-domain approach achieves lower latency for arrays of practical size, highlighting notable advantages of the proposed method in meeting real-time processing requirements.

Abbreviations

CB	:	Conventional Beamformer
CRLB	:	Cramér-Rao Lower Bound
CW	:	Continuous Wave
DF	:	Directivity Factor
DOA	:	Direction of Arrival
DS	:	Delay-and-Sum
FB	:	Feedback Beamformer
FFT	:	Fast Fourier Transform
FIM	:	Fisher Information Matrix
IIR	:	Infinite Impulse Response
ML	:	Maximum-Likelihood
MUSIC	:	Multiple Signal Classification
PSR	:	Peak-to-Sidelobe Ratio
RADAR	:	Radio Detection And Ranging
RIS	:	Reconfigurable Intelligent Surface
ULA	:	Uniform Linear Array

Notations

$x(t)$	Time-domain continuous input signal.
$x[m]$	Time-domain discrete input signal.
$X(F)$	Frequency-domain continuous input signal.
c	Speed of light.
d	Distance to target.
θ_d	Geometrical angle.
δ	Sensors' array inter-element spacing.
\mathbf{v}	A vector.
\mathbf{v}_i	The i -th element of vector \mathbf{v} .
\mathbf{v}^T	Transpose of vector \mathbf{v} .
\mathbf{v}^H	Hermitian transpose of vector \mathbf{v} .
\mathbf{A}	A matrix.
$\mathbf{A}_{i,j}$	The i, j -th element of matrix \mathbf{A} .
\mathbf{A}^T	Transpose of matrix \mathbf{A} .
\mathbf{A}^{-1}	Inverse of matrix \mathbf{A} .
$\text{tr}(\mathbf{A})$	Trace of matrix \mathbf{A} .

Chapter 1

Introduction

1.1 Background and Motivation

Array signal processing has profound applications across RADAR and sonar systems [1], [2], [3], smart antennas for satellite and cellular communications [4], [5], [6], [7], [8], automotive RADAR [9], [10], the early detection of diseases using medical imaging [11], [12], and recently, reconfigurable intelligent surface (RIS) applications [7], [13], [14].

Source localization is fundamentally a parameter estimation problem and constitutes a central component of spatial signal processing. It relies on sensor arrays to detect and characterize the origin of impinging signals in diverse environments [15]. The primary objective is to infer the unknown DOA or spatial position of a source based on the statistical and structural properties of the received array observations. This process starts with a reference actuator emitting signals into space while the sensor array captures reflections from various sources. By analyzing the time delays between the readings of these sensors, it is possible to estimate the exact location of the source accurately.

In far-field scenarios, source localization is commonly formulated as a DOA estimation problem. Under this formulation, the objective is to estimate the angular position of the source based on the spatial structure of the received array signals. Many approaches rely on the covariance matrix of the array data and exploit its subspace structure. Among the most prominent algorithms in this domain is the MUSIC (Multiple Signal Classification) algorithm [16], which leverages the orthogonality between the signal and noise subspaces of the covariance matrix to achieve high-resolution estimation. Another well-established technique is the ESPRIT (Estimation of Signal Parameters via Rotational Invariance Techniques) algorithm [17], which exploits the rotational invariance property between subarrays to directly compute the DOAs, thereby avoiding the spectral search required by MUSIC.

Another source localization technique is time difference of arrival (TDOA), which estimates the position of a signal source by measuring the differences in the arrival times of the signal at multiple spatially separated sensors [18]. By exploiting the measured

time delays, which are directly related to the source’s relative distance to each sensor, one can formulate hyperbolic equations that define the locus of possible source positions. Specifically, for two sensors located at \mathbf{p}_i and \mathbf{p}_j , the range difference equation is given by

$$\|\mathbf{p} - \mathbf{p}_i\| - \|\mathbf{p} - \mathbf{p}_j\| = c \Delta t_{ij},$$

which describes a branch of a hyperbola with the two sensors, where c is the propagation speed. The true source location is then estimated as the intersection of multiple such hyperbolic curves obtained from different sensor pairs, enabling accurate source localization.

A less practical, but asymptotically optimal in terms of achieving the Cramér–Rao lower bound (CRLB), are the Maximum Likelihood (ML) and Bayesian approaches to source localization [19], which tries to find the most probable DOA assuming prior information about the source distribution. These techniques rely on solving nonlinear optimization problems that often require iterative numerical procedures. While they provide a strong theoretical foundation and can outperform other estimators under ideal conditions, their high computational complexity, sensitivity to initialization, and risk of convergence to local minima make them less suitable for many practical real-time applications.

While source localization aims to estimate the positions of unknown emitters, its accuracy is inherently limited by noise, interference, and the spatial resolution of the array. Beamforming addresses these challenges by actively shaping the array’s response to enhance signals from desired directions while suppressing the influence of noise and interference from others [20]. This technique uses an array of sensors and determines the direction of the signal by weighing the inputs from each sensor. Choosing the right weight is crucial for optimizing the beamformer’s performance. In this way, beamforming serves as a complementary tool for localization: by improving the signal-to-noise ratio and isolating sources in space, it enables more precise estimation of their positions. When beamforming is implemented on digital platforms, it requires the discretization of the signal, which introduces quantization errors and necessitates a higher sampling rate. Because of these factors, research has focused on frequency-domain approaches [14], [21], [22], which require lower sampling rates and can benefit from the combined utilization of spectral and spatial data. However, the time domain is still an important area for development [3], [7], [12], [23], [24], particularly for applications that require low latency [24], such as real-time communication [3], [12]. In such cases, the time-domain approach can reduce computational complexity and execution time, even with a limited number of sensors.

Time-domain beamforming is particularly important for practical applications. Frequency-domain implementations require Fourier transforms and block-based processing, which can significantly increase computational load and introduce latency in

real-time systems. In contrast, time-domain methods operate directly on the incoming signal, enabling faster response. Moreover, continuous-wave (CW) signals simplify analysis but are rarely practical for real-time pulse radar systems, where wideband pulses contain many frequency components that further increase processing time in frequency-domain approaches. By working in the time domain, the beamformer can efficiently handle such signals, maintaining low latency while achieving high spatial resolution.

A common and widely studied implementation of beamforming is based on ULA [25], [26], [27], due to their simple implementation and easy analysis. The design of a ULA, including the number of elements and their spacing, significantly impacts its performance, affecting the sharpness of the mainlobe and sidelobe levels.

1.2 Overview of the Thesis

In this thesis, we propose a new architecture for a time-domain feedback-based beamformer to meet real-time processing demands. The feedback implemented in the architecture acts as a spatial IIR filter by integrating retransmission of the incoming signal while refraining from temporal processing of the signal and preserving a low-complexity array design.

At the outset of this research, the growing interest in feedback-based beamforming—driven by its potential for real-time operation—highlighted the need for highly efficient and low-latency implementations. This realization prompted a focused investigation into optimized beamforming strategies, ultimately steering the work toward the development and analysis of time-domain architectures as a compelling and practical solution.

Second, we have conducted a comprehensive time-domain analysis in the spatial processing field which led us to a theoretical framework and a closed-form solution for a time-domain feedback-based beamformer. This new architecture extends the current beamforming applications and provides an efficient way of implementing feedback mechanisms in beamforming systems. The array configuration is systematically derived, with key parameters—such as coefficient selection—determined through the application of the Fisher Information Matrix (FIM). A detailed analysis of the spatial characteristics confirms that the targeted recursive spatial response is attainable. Furthermore, the benefits of the proposed approach are articulated within the context of classical analytical frameworks, compared to commonly used conventional beamformers (CB), reinforcing its theoretical soundness and practical relevance.

Additionally, we conducted a comparative analysis of the proposed architecture implemented in both the time and frequency domains. This comparison was aimed at evaluating the advantages and limitations of the time-domain approach, ultimately demonstrating its feasibility for real-time implementation.

The overarching objective of this research is to deliver valuable insights, novel

methodologies, and practical implementations that markedly improve the performance and real-world applicability of feedback beamforming, especially in real-time applications where low latency is critical. This work aspires to offer a comprehensive and impactful advancement in the understanding, analysis and development of time-domain feedback beamforming.

1.3 Main Contributions

The primary contributions of this work include:

- A novel beamforming architecture incorporating feedback mechanisms has been developed, providing a comprehensive framework for the integration of feedback into beamforming systems. This work presents both a theoretical foundation and a closed-form solution for a time-domain feedback-based beamformer. It is important to recognize that the initial signal may originate either from the array or the target. In the subsequent discussion, we focus on the scenario in which the array initiates the transmission.
- An extensive analysis has been conducted to compare time-domain feedback beamforming with conventional time-domain approaches, emphasizing their respective advantages and limitations.

1.4 Thesis Organization

The thesis is systematically organized to ensure a coherent and thorough presentation of the research. The chapters are organized as follows:

Chapter 2 establishes the theoretical basis for the study. This chapter introduces the fundamental concepts underlying the research, including array processing, beamforming, and propagating wave fields. In addition, the principles of spatial and temporal processing are presented to establish the necessary background and to frame the motivation for the work carried out in this thesis.

Chapter 3 delves into the design and extensive analysis of the feedback beamformer, supported by simulations regarding key performance metrics, highlighting the advancements and efficiencies achieved by our approach. Additionally, a comparative analysis was conducted between the time-domain and frequency-domain implementations of the proposed FB architecture.

Chapter 4 presents a discussion of the results and summarizes the key findings. It concludes with suggestions for potential directions for future research.

Chapter 2

Preliminaries

This chapter presents the foundational concepts and mathematical tools that underpin the research in this thesis. The aim is to provide a self-contained overview of the essential background required for understanding the methods and analyses developed in the subsequent chapters. Key topics include signal sampling theory, sensor array configurations, spatial signal processing principles, and relevant mathematical representations. The material is selected to establish a clear theoretical basis and notation framework that will be used throughout the thesis.

2.1 Shannon’s Sampling Theorem

The Shannon Sampling Theorem, formulated by Claude E. Shannon in his influential 1949 paper “*Communication in the Presence of Noise*” [28], establishes the fundamental criterion under which a continuous-time signal can be completely represented by its discrete samples. Specifically, if a signal $x(t)$ is band-limited to a maximum frequency f_{\max} , meaning that its Fourier transform $X(f)$ satisfies $X(f) = 0$ for all $|f| > f_{\max}$, then the signal can be perfectly reconstructed from its samples $x(nT_s)$ taken at uniform intervals $T_s \leq \frac{1}{2f_{\max}}$. The minimum sampling frequency $f_s = \frac{1}{T_s}$ required for perfect reconstruction is known as the Nyquist rate and must satisfy $f_s \geq 2f_{\max}$.

Under these conditions, the original signal can be reconstructed using the Whittaker–Shannon interpolation formula:

$$x(t) = \sum_{n=-\infty}^{\infty} x(nT_s) \cdot \operatorname{sinc}\left(\frac{t - nT_s}{T_s}\right), \quad (2.1)$$

where $\operatorname{sinc}(x) = \frac{\sin(\pi x)}{\pi x}$ is the normalized sinc function. This expression illustrates that the continuous-time signal is a weighted sum of shifted sinc functions centered at each sample point. Each sample contributes to the reconstruction of the entire signal, and no information is lost in this representation provided the sampling theorem’s conditions are met.

The implications of Shannon’s result are profound. It provides the theoretical foun-

dation for the conversion of analog signals into digital form. The theorem assures that continuous signals, when sampled appropriately, can be transmitted, and processed digitally without any loss of information due to discretization.

Although Shannon’s formulation assumes ideal conditions—such as perfect band-limiting, infinite time support, and noiseless sampling—it remains a fundamental benchmark in both theory and practice. In real-world applications, where signals are only approximately band-limited and other imperfections exist, the sampling theorem still provides critical guidance for system design.

2.2 Sensor Arrays

Sensor arrays are a set of multiple, independent, spatially distributed sensing elements that work collaboratively to measure physical phenomena such as sound, electromagnetic waves, or mechanical vibrations. By leveraging the differences in the signals received at each sensor, relative to one reference sensor, across the array—such as time delays, phase shifts, or amplitude variations—sensor arrays enable advanced spatial signal processing techniques, including DOA estimation, beamforming, and source localization. These arrays play a central role in various domains such as RADAR, sonar, wireless communications, audio processing, and medical imaging. Their capacity to capture both spatial and temporal characteristics of signals makes them indispensable tools for detailed environmental analysis and source detection.

Sensor arrays can be configured in various geometric arrangements depending on the application requirements and physical constraints. Common configurations include ULA, where sensors are placed along a straight line; planar arrays and circular or spherical arrays, which offer uniform angular coverage in multiple dimensions. In ULA, the distance between any two consecutive sensors is denoted by δ . Considering an array of N elements, the location of the n -th sensor is denoted by

$$p_n = n\delta, \quad n = 0, \dots, N - 1. \quad (2.2)$$

The structure of an ULA with N elements and spacing of δ between is shown in Figure 2.1. The choice of configuration affects the array’s spatial resolution, sensitivity, and field of view. Factors such as inter-element spacing, aperture size, and array symmetry play a critical role in determining performance characteristics like beamwidth, sidelobe levels, and the ability to resolve multiple sources- key performances measures.

2.3 Beamforming

A beamformer is a signal processing system that operates alongside an array of sensors to achieve directional selectivity in the spatial domain. The array captures samples

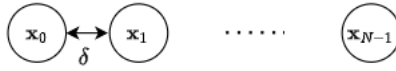


Figure 2.1 A ULA of N elements and inter-element spacing of δ .

of the wave field across different sensor positions, providing spatial information about the incoming signals. The beamformer processes these measurements with the goal of isolating the contribution from a specific direction of interest, even in the presence of noise and other sources. By exploiting differences in the spatial characteristics of the signals, beamforming enables the separation of sources that share similar spectral content but originate from distinct locations.

Let $x_n(t)$ denote the signal received at the n -th sensor of an N -element array. These signals can be stacked into the vector

$$\mathbf{x}(t) = [x_1(t) \ x_2(t) \ \cdots \ x_N(t)]^T.$$

The beamformer applies a set of complex weights $\mathbf{w} \in \mathbb{C}^N$ to form the output

$$y(t) = \mathbf{w}^H \mathbf{x}(t),$$

Proper selection of \mathbf{w} steers the array towards a desired direction while attenuating signals from other locations.

2.4 Temporal Digital Filtering Analogy to Spatial Signal Processing

A fundamental building block in many signal processing systems is the digital filter, a discrete-time implementation of filtering concepts that originated in analog systems. Over the years, digital filter design, a comprehensive research field, has evolved into a mature and well-established discipline. An FIR filter, as presented in Figure 2.2, has limited memory determined by the number of taps in the filter's configuration.

The subsequent discussion presents the ULA from a spatial filtering perspective, analogous to the operation of a temporal FIR filter [20]. In this interpretation, the DOA corresponds to temporal frequency, and CB [29] emerges as the spatial equivalent of FIR filtering in the temporal domain.

For a narrowband plane wave with DOA of θ_d , relative to the broadside direction of the array, the signal at the n -th sensor can be expressed as:

$$x_n(t) = s(t - \tau_n), \quad n = 0, 1, \dots, N - 1, \quad (2.3)$$

where $\tau_n = \frac{n\delta \sin \theta}{c}$ corresponds to the relative time delay between the n -th sensor and the designated reference sensor. The beamformer output is then

$$y(t) = \sum_{n=0}^{N-1} w_n x_n(t), \quad (2.4)$$

which mirrors the FIR filtering operation

$$y[k] = \sum_{n=0}^{N-1} h[n] x[k - n], \quad (2.5)$$

where w_n and $h[n]$ act as spatial and temporal filter coefficients, respectively. In both cases, the filter coefficients control the response, allowing systematic design techniques from digital filter theory to be adapted for array pattern synthesis.

While FIR filters are characterized by a finite-duration impulse response determined by the number of taps, IIR filters exhibit an impulse response of theoretically unbounded length. This property arises from the presence of feedback terms in their difference equations, allowing past output values to influence future outputs, as in Figure 2.3.

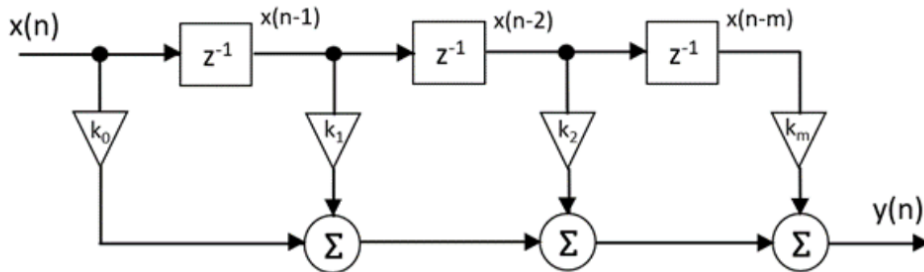


Figure 2.2 An FIR filter applied to signal x with coefficients k , generating a filtered signal y .

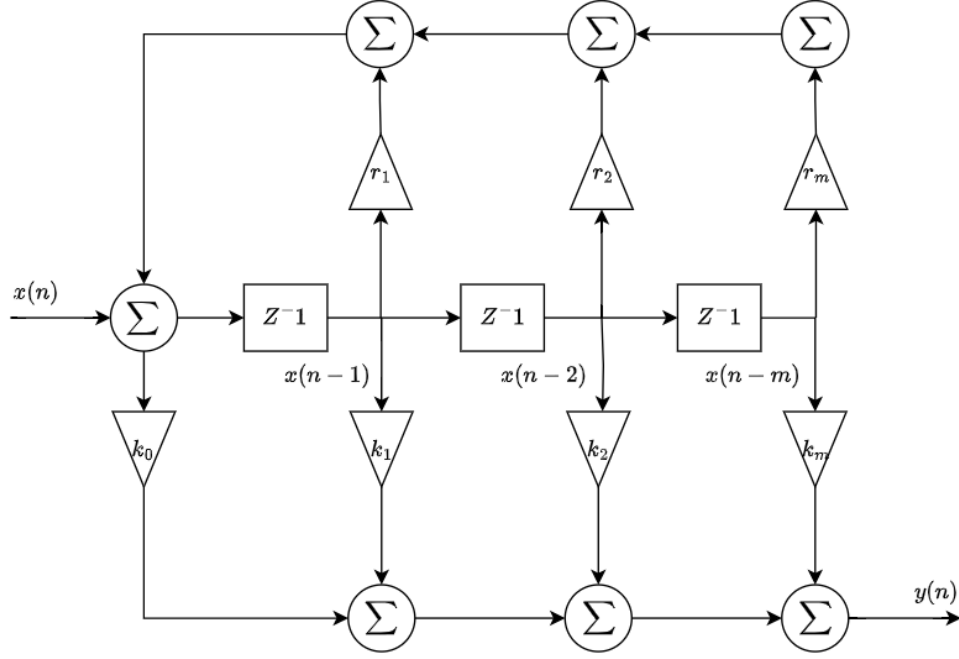


Figure 2.3 IIR filtering of the input signal x using feedforward coefficients k and a recursive component defined by coefficient r , producing the output signal y .

2.5 Propagating Wave Fields

Wave-field propagation provides a fundamental physical phenomenon and mathematical framework for understanding how physical quantities such as pressure, electric, or magnetic fields vary in space and time. These wave phenomena are governed by partial differential equations that describe how energy propagates through a medium. Wave spatial location is presented by Cartesian coordinates (x, y, z) , or spherical coordinates (r, θ, ϕ) , where $0 \leq \phi \leq 2\pi$, $0 \leq \theta \leq \pi$ are the azimuth and elevation angles, respectively. For simplicity and analytical tractability, we consider two-dimensional (2D) wave propagation.

Let t denote time, and assume a homogeneous, non-dispersive, and ideal (lossless) medium, the time-space representing the scalar wave equation in 2D is given by:

$$\nabla^2 \psi(\mathbf{r}, t) - \frac{1}{c^2} \frac{\partial^2 \psi(\mathbf{r}, t)}{\partial t^2} = \nabla^2 \psi(x, y, t) - \frac{1}{c^2} \frac{\partial^2 \psi(x, y, t)}{\partial t^2} = 0, \quad (2.6)$$

where ∇ is the Laplacian operator, $\psi(\mathbf{r}, t)$ is a scalar wave field, $\mathbf{r} = [x, y]^T \in \mathbb{R}^2$, and c is the propagation speed in the medium.

Assuming a time-harmonic solution of the form $\psi(\mathbf{r}, t) = \Re\{\phi(\mathbf{r})e^{j\omega t}\}$, substitution yields the 2D Helmholtz equation:

$$\nabla^2 \psi(\mathbf{r}, t) + k^2 \psi(\mathbf{r}, t) = 0, \quad (2.7)$$

where $k = \omega/c$ is the wave number.

A common solution to the Helmholtz equation in homogeneous media is the 2D plane wave:

$$\psi(\mathbf{r}, t) = Ae^{j(\omega t - \mathbf{k} \cdot \mathbf{r})}, \quad (2.8)$$

where A is the complex, constant amplitude, and $\mathbf{k} \in \mathbb{R}^2$ is the wave vector and is given by

$$\mathbf{k} = \begin{bmatrix} k_x \\ k_y \end{bmatrix} = k \begin{bmatrix} \cos \theta \\ \sin \theta \end{bmatrix}, \quad (2.9)$$

with θ denoting the DOA measured from the x -axis.

In the context of a sensor array composed of N elements located at positions $\mathbf{r}_n \in \mathbb{R}^2$, the response of the n -th element to a plane wave arriving from direction θ is:

$$\phi_n(\theta) = Ae^{-j\mathbf{k}^T \mathbf{r}_n}. \quad (2.10)$$

The complete array response can be written in vector form as:

$$\boldsymbol{\phi}(\theta) = A \cdot \mathbf{a}(\theta), \quad (2.11)$$

where $\mathbf{a}(\theta) \in \mathbb{C}^{N \times 1}$ is the *array steering vector* defined by:

$$\mathbf{a}(\theta) = \begin{bmatrix} e^{-j\mathbf{k}^T \mathbf{r}_1} \\ e^{-j\mathbf{k}^T \mathbf{r}_2} \\ \vdots \\ e^{-j\mathbf{k}^T \mathbf{r}_N} \end{bmatrix}. \quad (2.12)$$

Vector Field Formulation (Electromagnetic Waves)

In the case of vector wave fields, such as electromagnetic waves, the electric field $\mathbf{E}(\mathbf{r}, t)$ satisfies the vector wave equation:

$$\nabla^2 \mathbf{E}(\mathbf{r}, t) - \mu\epsilon \frac{\partial^2 \mathbf{E}(\mathbf{r}, t)}{\partial t^2} = 0, \quad (2.13)$$

where μ and ϵ are the permeability and permittivity of the medium, respectively.

Assuming time-harmonic behavior, the field can be written as $\mathbf{E}(\mathbf{r}, t) = \Re\{\mathbf{E}(\mathbf{r})e^{j\omega t}\}$, yielding the Helmholtz equation for each Cartesian component:

$$\nabla^2 \mathbf{E}(\mathbf{r}) + k^2 \mathbf{E}(\mathbf{r}) = 0. \quad (2.14)$$

Each component of the vector field obeys a scalar wave equation, enabling the application of array steering and beamforming principles component-wise when polarization is not considered.

Green's Function and Point Sources in 2D

The free-space Green's function in 2D for a point source located at \mathbf{r}_0 is given by:

$$G(\mathbf{r}, \mathbf{r}_0) = \frac{j}{4} H_0^{(2)}(k |\mathbf{r} - \mathbf{r}_0|), \quad (2.15)$$

where $H_0^{(2)}(\cdot)$ is the zero-order Hankel function of the second kind, representing an outgoing cylindrical wave. In the far-field region, this approximates to [30]:

$$G(\mathbf{r}, \mathbf{r}_0) \approx \sqrt{\frac{1}{8\pi k |\mathbf{r}|}} e^{-jk|\mathbf{r}|} e^{jk\hat{\mathbf{r}} \cdot \mathbf{r}_0}. \quad (2.16)$$

This approximation highlights the plane wave behavior of spherical waves in the far-field and justifies the use of steering vectors in array signal processing.

2.6 Array Performance in the Spatial Domain

2.6.1 Beampattern

A beampattern characterizes the spatial sensitivity of a sensor array as a function of DOA. It describes how the array responds to signals arriving from different angles, effectively illustrating the array's ability to focus or attenuate energy in specific directions. The shape of the beampattern is determined by factors such as the array geometry, the weighting applied to the elements, and the frequency of the incoming signal. In general, when dealing with 3D space, the DOA depends on two angles- azimuth and elevation. Nonetheless, to simplify we consider a 2D planar DOA (azimuth without elevation), thus the beampattern is expressed as a function of the angle θ :

$$B(\theta) = |Z(\theta)|, \quad (2.17)$$

where $Z(\theta)$ is the output of the beamformer. In the context of beamforming, the beampattern is a key tool for visualizing and analyzing the directional properties of the array response, including features such as the mainlobe, sidelobes, and nulls. The beampattern is typically presented graphically on a logarithmic scale, as shown in Figure 2.4.

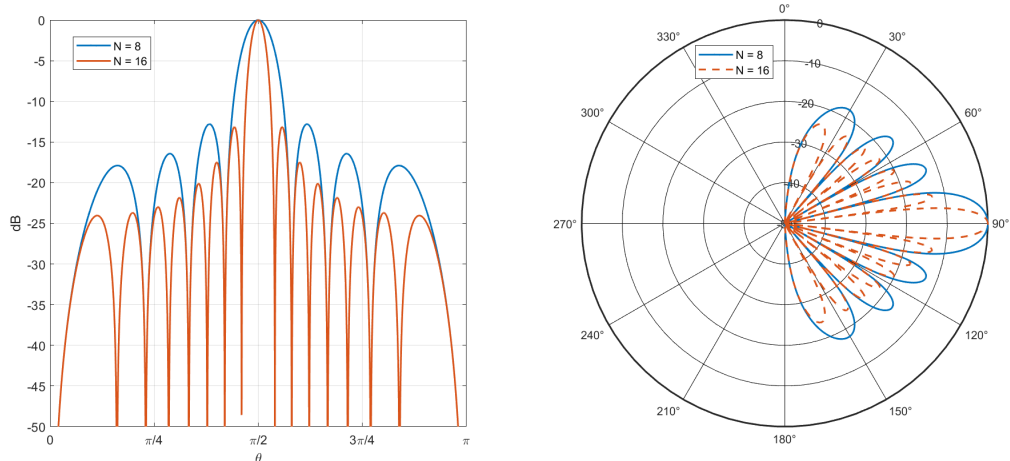


Figure 2.4 Two widely used methods are employed to visualize the 2D planar beam-pattern. Both plots illustrate the responses of 8-element and 16-element conventional beamformers, shown in blue and orange, respectively. On the left, the response is displayed over the $[0, \pi]$ angular range in decibels (dB). On the right, a polar plot presents the same response in dB, with the DOA expressed in degrees.

2.6.2 The Normalized Beampattern

The system-dependent nature of absolute gain prevents meaningful comparison between beampatterns with differing mainlobe peak values. Therefore, the normalized beampattern is a standardized representation of the spatial response of an array, scaled relative to its maximum value. By dividing the beampattern by its peak magnitude, the mainlobe's output gain at its peak is 1 ($0dB$). This form will hereafter be referred to as:

$$H_{\text{norm}}(\theta) = \frac{H(\theta)}{H(\theta_s)}, \quad (2.18)$$

where H is the array's response and θ_s is the DOA toward which the array is steered. The resulting normalized pattern emphasizes the relative gain across different directions, independent of absolute power levels.

2.6.3 Peak-to-Sidelobe Ratio

A well-known parasitic effect in beampatterns is the presence of sidelobes, which appear as secondary energy peaks outside the mainlobe. These sidelobes are generally most prominent near the mainlobe and gradually diminish toward the periphery of the beampattern. One of the key performance metrics used to evaluate the quality of a beampattern is the Peak-to-Sidelobe Ratio (PSR). It is defined as the ratio between the maximum value of the mainlobe and the highest sidelobe level in the beampattern. A high PSR indicates strong spatial selectivity, meaning the array is highly focused in the desired direction while effectively suppressing responses from other directions.

Improving the PSR often involves trade-offs with other parameters, such as beamwidth or robustness to model mismatch. The PSR can be expressed as:

$$\text{PSR} = \frac{|B(\theta_s)|}{\max_{\theta \neq \theta_s} |B(\theta)|} \quad (2.19)$$

2.6.4 Directivity

Directivity is a fundamental measure used to quantify the directional concentration of an array's radiated or received power. It expresses how focused the beam is in a particular direction compared to an isotropic radiator, which distributes energy equally in all directions. Additionally, for a receiving array, the denominator corresponds to the noise power at the array output caused by isotropic noise. Mathematically, directivity $D(\theta_s)$ is defined as the ratio of the power density in the steering DOA (θ_s) to the average power density radiated over all directions. For an array with beampattern $B(\theta)$, the power pattern for some DOA (θ_s) is defined as $P(\theta_s)$, to be the squared magnitude of the beampattern $B(\theta_s)$

$$P(\theta_s) = |B(\theta_s)|^2. \quad (2.20)$$

The directivity can thus be expressed as

$$D(\theta_s) = \frac{|B(\theta_s)|^2}{\frac{1}{2\pi} \int_0^{2\pi} |B(\theta)|^2 d\theta} = \frac{P(\theta_s)}{\frac{1}{2\pi} \int_0^{2\pi} P(\theta) d\theta} \quad (2.21)$$

where the denominator represents the average power over the angular domain. A higher directivity indicates better spatial selectivity, allowing the system to focus energy more narrowly.

Chapter 3

Time-Domain Feedback Beamforming: Model and Design

This chapter presents the core contribution of this thesis, which focuses on the development of a time-domain formulation for feedback beamforming. Building on the theoretical foundations laid out in the Preliminaries, the research introduces a novel analytical expression for the temporal response of an array-based feedback system. Furthermore, an optimization framework was developed to compute the weight coefficients that yield the desired spatio-temporal beampattern. The results provide both theoretical insight and practical tools for controlling and analyzing wavefield responses in the time domain. Section 3.1 provides a detailed exposition of the time-domain feedback-based beamforming concept. Section 3.2 then presents the application of information-theoretic principles in the array processing context. In Section 3.3, the performance of the proposed beamformer is evaluated using standard beamforming metrics. Finally, Section 3.4 offers a comprehensive comparison between the time- and frequency-domain implementations of feedback beamforming.

3.1 Problem, Signal Model and Notations

In this section, we introduce a feedback-based spatial signal processing architecture operating in the time domain. While the concept is inspired by prior designs formulated in the frequency domain, our goal is to adapt it for time-domain applications, which are more appropriate for real-time scenarios. The proposed architecture, illustrated in Figure 3.2, utilizes two sets of weights: β to generate the output signal $z(t)$, and α to construct the transmitted feedback signal (T_x). These two components are implemented using independently designed beamformers. The system is driven by an external signal $s(t)$, and additive noise $n(t)$ is assumed to be present at the environment. It is worth noting that when the feedback weights are disabled (i.e., $\alpha = \mathbf{0}$), the architecture reduces to a CB. The feedback loop is indicated by a dashed block labeled FB for reference in later sections.

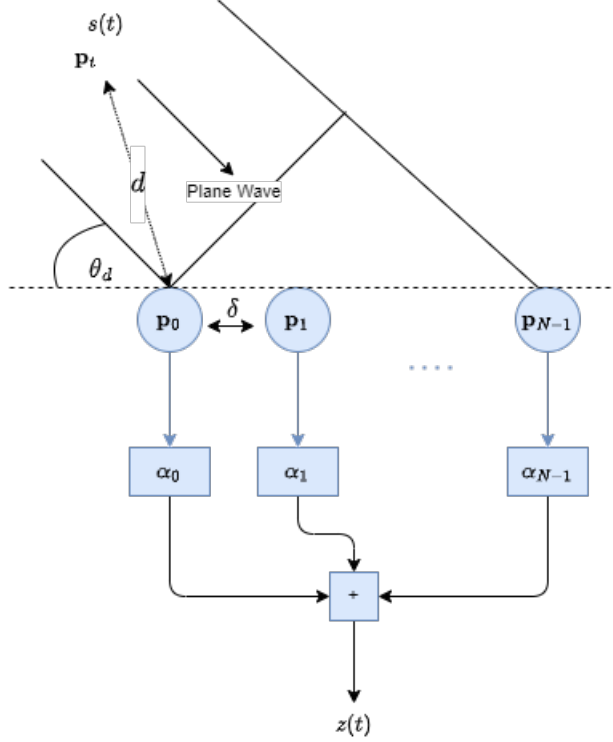


Figure 3.1 A spatial reference system illustrating the relationship between Cartesian and spherical coordinates in two dimensions.

In this chapter, we next present the N -element ULA beamforming architecture and its resemblance to FIR filters, as discussed in Section 2.4. The location of the n -th sensor is denoted by \mathbf{p}_n for $n = 0, \dots, N - 1$, with \mathbf{p}_0 representing the reference point relative to a stationary target positioned at \mathbf{p}_t . For simplicity, we consider a two-dimensional formulation. The DOA of the reflected signal, relative to the broadside direction of the array, is denoted as θ_d . The distance from the reference sensor to the target is given by $d = |\mathbf{p}_0 - \mathbf{p}_t|$. The configuration of ULA is depicted in Figure 3.1. The signal measured at the n -th sensor is given by

$$x_n(t) = g_c s(t - \tau_{pd} - \tau_n) + v_n(t), \quad (3.1)$$

where g_c is the channel gain, τ_{pd} is the propagation delay from the target to the reference sensor and back, given by $\tau_{pd} = \frac{2d}{c}$ and $v_n(t)$ is the noise at the n -th sensor.

Following Shannon's sampling theorem in Section 2.1, under the assumptions of an ideal band-limited signal and sampling at a rate not lower than the Nyquist frequency, the continuous-time signal can be represented as

$$s(t) = \sum_{m=-\infty}^{\infty} s[m] \text{sinc}(tf_s - m) \quad (3.2)$$

where $f_s = \frac{1}{T_s}$ is the sampling frequency, $s[m] = s(mT_s)$ is the sampled signal and

$\text{sinc}(x) = \frac{\sin(\pi x)}{\pi x}$ and $\text{sinc}(x) = \frac{\sin(x)}{x}$ is the normalized and unnormalized sinc functions, respectively. Substituting (3.1) into (3.2), and under the assumption of a noiseless environment, where $v_n(t) = 0$ for all the sensors, we have

$$x_n(t) = g_c \sum_{m=-\infty}^{\infty} s[m] \text{sinc}((t - \tau_{\text{pd}} - \tau_n)f_s - m). \quad (3.3)$$

The discrete-time signal measured in the n -th sensor can be written as

$$\begin{aligned} x_n[m] &= x_n(mT_s) \\ &= g_c \sum_{m'=-\infty}^{\infty} s[m'] \text{sinc}((mT_s - \tau_{\text{pd}} - \tau_n)f_s - m') \\ &= g_c \sum_{l=-\infty}^{\infty} s[m-l] \text{sinc}(l - (\tau_{\text{pd}} + \tau_n)f_s). \end{aligned} \quad (3.4)$$

By following the framework presented in [31] for general analysis and by defining $\Delta = \tau_{\text{pd}}f_s$, we have

$$\begin{aligned} x_n[m] &= g_c \sum_{l=-\infty}^{\infty} s[m-l] \text{sinc}(l - \Delta - f_s\tau_n) \\ &\approx g_c \sum_{l=-P}^{P+L_h-1} s[m-l] \text{sinc}(l - \Delta - f_s\tau_n) \end{aligned} \quad (3.5)$$

where the summation is truncated around the mainlobe of the sinc function. The approximation in (3.5) holds for $P \in \mathbb{N}$ and $P - \Delta - f_s\tau_n \gg 1$. $L_h \in \mathbb{N}$ is the length of the FIR filter to be defined later. We can formulate (3.5) as

$$x_n[m] = g_c \mathbf{g}_n^T(\theta_d, d) \mathbf{s}[m] \quad (3.6)$$

where $\mathbf{s}[m]$ contains $L = 2P + L_h$ successive samples of the signal $s[m]$:

$$\mathbf{s}[m] = \left[s[m+P] \quad s[m+P-1] \quad \dots \quad s[m-P-L_h+1] \right]^T \quad (3.7)$$

and $\mathbf{g}_n(\theta_d, d)$ is given by

$$\mathbf{g}_n(\theta_d, d) =$$

$$\left[\text{sinc}(-P - \Delta - f_s\tau_n) \quad \text{sinc}(-P + 1 - \Delta - f_s\tau_n) \quad \dots \quad \text{sinc}(P + L_h - 1 - \Delta - f_s\tau_n) \right]^T. \quad (3.8)$$

Considering L_h successive time samples of the n -th sensor signal, (3.6) becomes a

vector of length L_h :

$$\begin{aligned}\mathbf{x}_n[m] &= [x_n[m] \quad x_n[m-1] \quad \dots \quad x_n[m-L_h+1]]^T \\ &= g_c \mathbf{G}_n(\theta_d, d) \mathbf{s}[m]\end{aligned}\quad (3.9)$$

where $\mathbf{G}_n(\theta_d, d)$ is a Toeplitz matrix of size $L_h \times L$ with

$$[\mathbf{G}_n(\theta_d, d)]_{ij} = \text{sinc}(-P - i + j - \Delta - f_s \tau_n) \quad (3.10)$$

where $i = 0, \dots, L_h - 1$ and $j = 0, \dots, L - 1$. By combining the samples from the N sensors, we get a vector of length NL_h :

$$\begin{aligned}\mathbf{x}[m] &= [\mathbf{x}_0[m]^T \quad \mathbf{x}_1[m]^T \quad \dots \quad \mathbf{x}_{N-1}[m]^T]^T \\ &= \mathbf{G}(\theta_d, d) \mathbf{s}[m]\end{aligned}\quad (3.11)$$

where $\mathbf{G}(\theta_d, d)$ is a matrix of size $NL_h \times L$:

$$\mathbf{G}(\theta_d, d) = \begin{bmatrix} \mathbf{G}_0(\theta_d, d) \\ \mathbf{G}_1(\theta_d, d) \\ \vdots \\ \mathbf{G}_{N-1}(\theta_d, d) \end{bmatrix}. \quad (3.12)$$

The signal $\mathbf{x}[m]$ is affected by the array's geometry, represented by τ_n in each element of $\mathbf{G}(\theta_d, d)$. This is similar to the structure observed in the frequency-domain model. Therefore, the steering vector is the counterpart to $\mathbf{G}(\theta_d, d)$ in the frequency domain. This shows a direct relationship between time-domain signal processing and its frequency-domain equivalent through the array geometry.

3.1.1 Feedback Beamforming

This section discusses the feedback-based beamformer architecture used for spatial signal processing. The FB architecture is similar to an IIR-like filter. It uses a feedback loop to retransmit the signal $s_{\text{fb}}(t)$, which is synthesized from the weighted aggregation of sensor samples:

$$s_{\text{fb}}(t) = \sum_{k=0}^{N-1} \alpha_k x_k(t - \tau_{\text{pd}} - \tau_n).$$

This feedback loop creates a dynamic spatial processing environment, making it a novel approach for spatial signal processing. The details of this architecture are discussed in [22]. The architecture combines data collected by sensors and processes it through two weighted sums called $\boldsymbol{\alpha}$ and $\boldsymbol{\beta}$. In the time domain, L_h consecutive time samples are taken from each of the N sensors. $\boldsymbol{\alpha}$ and $\boldsymbol{\beta}$ are vectors with dimensions of

NL_h . These samples may contain desired signals and unwanted noise or interference from different directions. The system's output is denoted as $z(t)$ and is created using a weighted vector called β . The retransmitted signal combines the source signal and an additional weighted sum using the vector α . In order to demonstrate the presence of interference in this setup, Figure 3.2 introduces a noise source, \mathbf{n}_t , placed at an angle θ_n relative to the array's broadside. This configuration highlights the ability of the FB architecture to handle complicated signal environments by utilizing spatial feedback loops for improved signal processing.

By extending the signal model in (3.1) to the FB architecture and considering the noiseless case, the signal measured at the n -th sensor is as follows [22]:

$$\begin{aligned} x_n(t) &= g_c (s(t - \tau_{pd} - \tau_n) + s_{fb}(t)) \\ &= g_c \left(s(t - \tau_{pd} - \tau_n) + \sum_{k=0}^{N-1} \alpha_k x_k(t - \tau_{pd} - \tau_n) \right). \end{aligned} \quad (3.13)$$

By using Shannon's sampling theorem, as is the case in (3.5), the discrete-time signal can be written as -

$$x_n[m] \approx g_c \left[\sum_{l=-P}^{P+L_h-1} s[m-l] \text{sinc}(l - \Delta - f_s \tau_n) + \sum_{l=-P}^{P+L_h-1} \sum_{k=0}^{N-1} \alpha_k^T \mathbf{x}_k[m-l] \text{sinc}(l - \Delta - f_s \tau_n) \right] \quad (3.14)$$

where α_k is a vector of length L_h that defines the weights for the time samples of the k -th sensor:

$$\alpha_k = [\alpha_k[0] \quad \alpha_k[1] \quad \dots \quad \alpha_k[L_h - 1]]^T.$$

By simplifying the expression above, (3.14) can be rewritten as

$$x_n[m] = g_c \left\{ \sum_{l=-P}^{P+L_h-1} \left[\text{sinc}(l - \Delta - f_s \tau_n) \left(s[m-l] + \sum_{k=0}^{N-1} \alpha_k^T \mathbf{x}_k[m-l] \right) \right] \right\}. \quad (3.15)$$

Combining both (3.9) and (3.15) results in

$$\mathbf{x}_n[m] = g_c \mathbf{G}_n(\theta_d, d) [\mathbf{s}[m] + \mathbf{i}_\ell \alpha^T \mathbf{x}[m]] \quad (3.16)$$

where \mathbf{i}_ℓ is the ℓ -th column of the $L \times L$ identity matrix, \mathbf{I}_L , and α is a vector of length NL_h , consisting of the weights for all the samples. By unifying all the sensors together, we obtain

$$\mathbf{x}[m] = g_c \mathbf{G}(\theta_d, d) [\mathbf{s}[m] + \mathbf{i}_\ell \alpha^T \mathbf{x}[m]]. \quad (3.17)$$

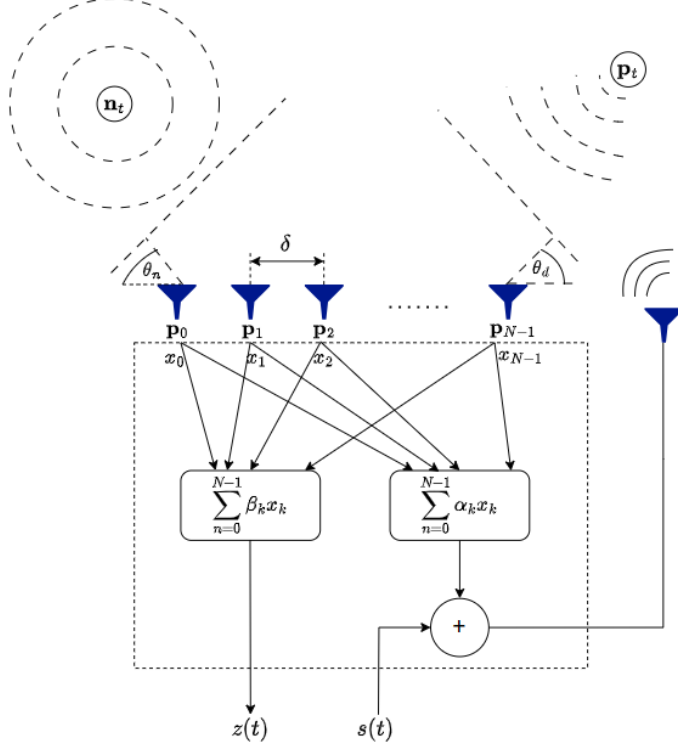


Figure 3.2 Proposed beamformer structure. The goal is to spatially localize the target, P_t , by retransmitting the signal.

The above can be simplified to

$$\left[1 - g_c \boldsymbol{\alpha}^T \mathbf{G}(\theta_d, d) \mathbf{i}_\ell\right] \mathbf{x}[m] = g_c \mathbf{G}(\theta_d, d) \mathbf{s}[m]. \quad (3.18)$$

Thus, the relation between the input signal and the sensors' samples is given by

$$\mathbf{x}[m] = \frac{g_c \mathbf{G}(\theta_d, d) \mathbf{s}[m]}{1 - g_c \boldsymbol{\alpha}^T \mathbf{G}(\theta_d, d) \mathbf{i}_\ell}. \quad (3.19)$$

Where $\mathbf{G}(\theta_d, d) \in \mathbb{R}^{NL_h \times L}$, $\mathbf{i}_\ell \in \mathbb{R}^L$. It is important to note that \mathbf{i}_ℓ denotes a selection vector that extracts the ℓ -th sample of $g_c \boldsymbol{\alpha}^T \mathbf{G}(\theta_d, d)$.

In principle, any element of the input vector signal $\mathbf{s}[m]$ can be considered the desired signal. Moreover, based on the proposed feedback beamforming architecture, the output of the beamformer can be represented as $z[m] = \boldsymbol{\beta}^T \mathbf{x}[m]$. Therefore, the relationship between the input signal and FB output can be expressed as follows:

$$H_{\beta, \alpha} \triangleq \frac{z}{s} = \frac{g_c \boldsymbol{\beta}^T \mathbf{G}(\theta_d, d) \mathbf{i}_\ell}{1 - g_c \boldsymbol{\alpha}^T \mathbf{G}(\theta_d, d) \mathbf{i}_\ell}. \quad (3.20)$$

As will be shown, in contrast to conventional beamforming approaches (i.e., without feedback), the proposed feedback-based architecture extends the effective aperture of the array, thereby achieving reduced beamwidth and superior sidelobe attenuation.

These improvements arise from its recursive structure, where the weights α and β provide additional degrees of freedom for shaping the spatial response. By appropriately tuning these parameters, the beamformer can be designed to exhibit highly directive patterns with controllable characteristics.

After analyzing both the time-domain response and the frequency-domain response outlined in [22], it is apparent that they are closely related. The steering vector utilized in the frequency domain is similar to the construct $\mathbf{G}(\theta_d, d)\mathbf{i}_\ell$ in the time domain. Additionally, the phase shift component $e^{-j\phi}$ in the frequency domain is comparable to fine-tuning the interpolation matrix $\mathbf{G}(\theta_d, d)$ in the time domain by adjusting the propagation delay associated with the target's range estimation. Thus, this adjustment shows the alignment between time-domain processing and its frequency-domain counterpart by manipulating the coefficient interpolation matrix.

3.2 Fisher Information Matrix

The optimal selection of the beamformer weights is a crucial factor in its performance. Unfortunately, even slight deviations from optimal weights may significantly impact beamformer efficacy, a concept that will be further explored in the subsequent sections. When compared to a CB, the unique aspect of the feedback beamformer is the introduction of spatial feedback through the retransmitted signal. This retransmission adds a layer of complexity and potential for enhanced performance by incorporating additional system information, as detailed in [22]. The efficacy of the FB hinges on the precise estimation of the DOA (θ_d) and the target's range (d). There are several ways to assess the estimations' accuracy. One potential method of determining the provided feedback mechanism's impact is quantifying the system's supplementary information. To this end, the CRLB was used, leveraging the FIM. Given that the analysis and development of the beamformer's response are conducted within the time domain, we utilized the time-domain FIM to evaluate the performance potential of the FB system.

The (m, n) -th FIM element is given by [32]

$$[\mathbf{J}(\zeta)]_{m,n} = \left| \frac{\partial z(\zeta)}{\partial \zeta_m} \right|^T \mathbf{R}^{-1}(\zeta) \left| \frac{\partial z(\zeta)}{\partial \zeta_n} \right| + \frac{1}{2} \text{tr} \left[\mathbf{R}^{-1}(\zeta) \frac{\partial \mathbf{R}(\zeta)}{\partial \zeta_m} \mathbf{R}^{-1}(\zeta) \frac{\partial \mathbf{R}(\zeta)}{\partial \zeta_n} \right] \quad (3.21)$$

where $\zeta = [\theta_d, d]$ represents the vector of the parameters, and $\text{tr}(\cdot)$ denotes the trace operation on a matrix. The variables $m, n \in 1, 2$ specify the estimated parameters, and $\mathbf{R}(\zeta)$ represents the $N \times N$ noise covariance matrix. By assuming the presence of white noise, which is statistically independent of the parameter vector ζ , and given that $z(t)$ is scalar, expression (3.21) can be simplified as

$$[\mathbf{J}(\zeta)]_{m,n} = \left| \frac{\partial z(\zeta)}{\partial \zeta_m} \right| \left| \frac{\partial z(\zeta)}{\partial \zeta_n} \right|. \quad (3.22)$$

The above derivatives yield the following main diagonal elements:

$$\begin{aligned} \mathbf{J}_{\theta_d\theta_d} &= \frac{f_1}{[1 - g_c \boldsymbol{\alpha}^T \mathbf{G}(\theta_d, d) \mathbf{i}_\ell]^4} \\ \mathbf{J}_{dd} &= \frac{f_2}{[1 - g_c \boldsymbol{\alpha}^T \mathbf{G}(\theta_d, d) \mathbf{i}_\ell]^4} \end{aligned} \quad (3.23)$$

where f_1 and f_2 are functions of the parameter set $\boldsymbol{\alpha}$, β , and $\mathbf{G}(\theta_d, d)$ and its partial derivatives. A detailed proof of (3.23) is given in Appendix B. In order to obtain the optimal and precise estimate, it is required to maximize the diagonal elements of the FIM, $J_{\theta_d\theta_d}$ and J_{dd} . This maximization is carried out by minimizing the denominator $|1 - g_c \boldsymbol{\alpha}^T \mathbf{G}(\theta_d, d) \mathbf{i}_\ell|$.

The optimal weight $\boldsymbol{\alpha}$ can be written as

$$\boldsymbol{\alpha}_{\text{opt}}^T = \frac{1}{\hat{g}_c} \mathbf{i}_\ell^T \mathbf{G}^T(\theta_d, d) \left[\mathbf{G}(\theta_d, d) \mathbf{G}^T(\theta_d, d) \right]^{-1} \quad (3.24)$$

where \hat{g}_c is the channel gain estimate. For simplicity, the output weight is $\beta = \boldsymbol{\alpha}_{\text{opt}}$. The optimal beamformer weights vector contains the exact values for the DOA and the target range, which, in practice, are unknown. Thus, the optimal weights, considering both the DOA estimate $\hat{\theta}_d$ and the range estimate \hat{d} , are

$$\boldsymbol{\alpha}_{\text{opt}}^T = \beta_{\text{opt}}^T = \frac{1}{\hat{g}_c} \mathbf{i}_\ell^T \mathbf{G}^T(\hat{\theta}_d, \hat{d}) \left[\mathbf{G}(\hat{\theta}_d, \hat{d}) \mathbf{G}^T(\hat{\theta}_d, \hat{d}) \right]^{-1}. \quad (3.25)$$

Substituting (3.25) into (3.20) yields the optimal beamformer time response:

$$H_{\beta_{\text{opt}}, \boldsymbol{\alpha}_{\text{opt}}} = \frac{r \mathbf{i}_\ell^T \mathbf{G}^T(\hat{\theta}_d, \hat{d}) \left[\mathbf{G}(\hat{\theta}_d, \hat{d}) \mathbf{G}^T(\hat{\theta}_d, \hat{d}) \right]^{-1} \mathbf{G}(\theta_d, d) \mathbf{i}_\ell}{1 - r \mathbf{i}_\ell^T \mathbf{G}^T(\hat{\theta}_d, \hat{d}) \left[\mathbf{G}(\hat{\theta}_d, \hat{d}) \mathbf{G}^T(\hat{\theta}_d, \hat{d}) \right]^{-1} \mathbf{G}(\theta_d, d) \mathbf{i}_\ell} \quad (3.26)$$

where $r \triangleq \frac{g_c}{\hat{g}_c}$ is the channel gain error. It is important to note that when the denominator of the right-hand side of (3.26) tends to zero, the beamformer response becomes unbounded, indicating that the equivalent array would theoretically consist of infinitely many elements, achieving perfect spatial selectivity.

3.3 Beamformer Evaluation

In order to assess the beamformer's efficacy, it is essential to consider a range of architecture-specific (such as N and δ) and target-specific (such as the DOA and the target's distance from the array) parameters. This section examines the FB response, as detailed in (3.26), and evaluates its performance using key metrics such as sidelobe level reduction, directivity factor (DF), and beamwidth. These metrics are standard for assessing the performance of ULA beamformers. The examination was tested on the beampattern of the proposed beamformer, which is defined by $10 \log_{10} |H_{\beta_{\text{opt}}, \boldsymbol{\alpha}_{\text{opt}}}|^2$

in units of dB. The FB's performance metrics were benchmarked against conventional ULA beamformers, including the delay and sum (DS) and the maximum DF beamformers, which lack the FB's feedback mechanism. This comparative analysis will highlight FB's advancements and its potential impact.

3.3.1 Channel Gain Estimation Error

In the previous section, we defined the channel gain error as $r \triangleq \frac{\hat{g}_c}{g_c}$. In the following subsection, we will investigate the influence of different estimations of r on the proposed beamformer response. Figure 3.3 demonstrates the beampattern for several channel gain estimation errors. As can be seen in Figure 3.3, r represents the array aperture. The closer the value is to 1 (precise gain alignment), the narrower the mainlobe, and the better the sidelobe attenuation. It is noteworthy that when achieving precise gain matching (i.e., as r tends towards 1), the beamformer achieves impeccable spatial selectivity.

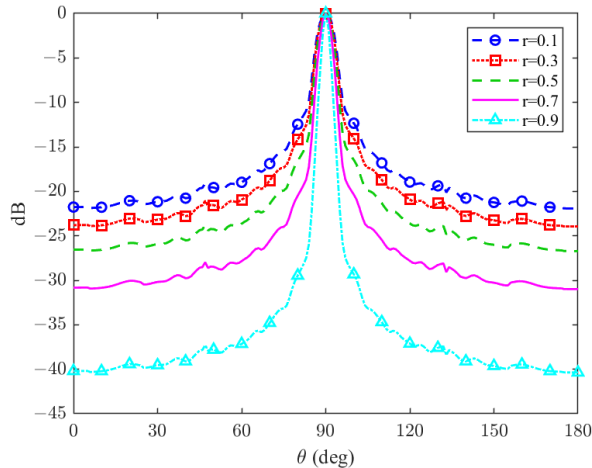


Figure 3.3 Feedback beamformer beampattern for different channel gain estimation errors for $\theta_d = 90^\circ$, $N = 10$ and $\delta = 1cm$.

In practice, the channel gain g_c may be estimated using pilot-based methods, in which a known training signal is transmitted and the received observations are used to form a least-squares or maximum-likelihood estimate of g_c from the signal model in (3.1).

3.3.2 Mainlobe and Sidelobe Attenuation

The accuracy of a beamformer is determined by the width of its center lobe and the height of its sidelobes. The behavior of a proposed feedback beamformer compared to the DS and maximum DF beamformers, which is presented in [31], is shown in Figure 3.4, depending on θ . To this end, we assume perfect range estimation, that is, $d = \hat{d}$. The DS beamformer is a basic beamformer obtained by the sum of the

time-shifted versions of the sensor signals. The maximum DF beamformer tends to narrow the mainlobe and attenuate the sidelobes. As demonstrated in Figure 3.4, the feedback beamformer beampattern has a much narrower mainlobe than the DS beamformer. Additionally, the feedback beamformer has about an order of magnitude better attenuation than the DS beamformer. Furthermore, the FB mainlobe is almost as narrow as the maximum DF beamformer mainlobe. This indicates that the beamformer filter is spatially effective, nearly as much as a beamformer explicitly designed for that purpose. Moreover, while the distortionless maximum DF beamformer is designed to have a narrow beamwidth, it comes at the cost of high sidelobes. The feedback beamformer closely matches the mainlobe beamwidth while having much better sidelobe attenuation. These results indicate that our proposed beamformer can achieve better localization estimation for two of the most common beamformer performance measures.

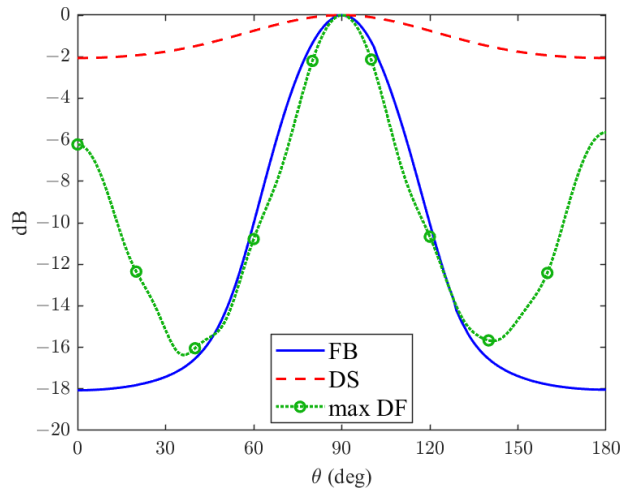


Figure 3.4 Feedback beamformer beampattern (blue line), compared to known ULA beamformers, DS (dashed red line), and maximum DF (dashed green line) respectively for $\theta_d = 90^\circ$, $r = 0.6$, $N = 10$ and $\delta = 1cm$.

3.3.3 Directivity Factor

The directivity factor is an important quality factor of the beamformer. It refers to the level of directionality of the beamformer. It is measured by the ratio between the beamformer gain in a specific direction and the average gain in all directions. In the time domain, it is defined as [31]

$$D[\boldsymbol{\alpha}, \boldsymbol{\beta}, \cos(\theta_d), d] = \frac{|B(\boldsymbol{\alpha}, \boldsymbol{\beta}, \cos(\theta_d), d)|^2}{\frac{1}{2\pi} \int_0^{2\pi} |B(\boldsymbol{\alpha}, \boldsymbol{\beta}, \cos(\theta), d)|^2 d\theta} \quad (3.27)$$

where B represents the beampattern. As explained and developed in [33], the DF for a generic ULA in far field with isotropic noise is

$$D = 2\frac{N\delta}{\lambda} \quad (3.28)$$

for broadside case, large values of N and $\lambda \gg \delta$.

Furthermore, as explained in detail in [22] and shown in Figure 3.3, the array aperture is a function of r . For $r = 0$, the standard ULA beamformer is obtained, while for increasing values of r , the array's aperture is increased. In order to avoid spatial ambiguities in the results of the directivity factor, $r = 0.6$ was used throughout the entire experiment. By simulating the DF for both the feedback beamformer architecture and generic ULA and plotting the result as a function of δ , in Figure 3.5, we show that the DF was significantly improved. In addition, it can be seen from Figure 3.5 that when the number of sensors is increased, or the distance between sensors is increased, the DF of both cases increases as well due to better spatial resolution.

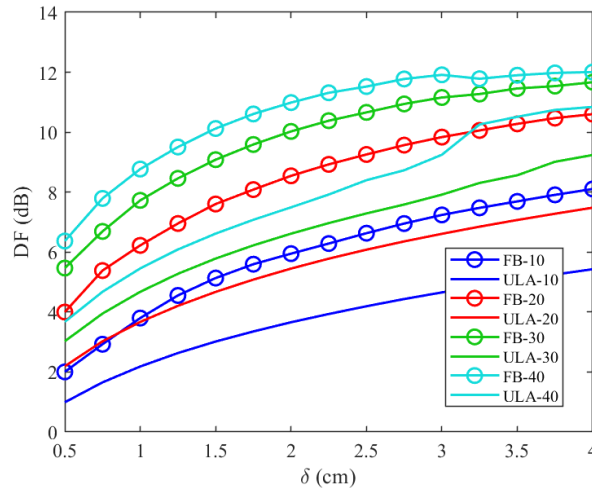


Figure 3.5 Directivity factor as a function of δ for the feedback beamformer (3.26) (lines with circles) compared to DF for a generic ULA (solid lines) for a signal wave with a frequency carrier of 1 GHz, $r = 0.6$, $\theta_d = 45^\circ$. DF was tested for several values of N : $N = 10$ (blue lines), $N = 20$ (red lines), $N = 30$ (green lines), and $N = 40$ (light blue lines).

3.3.4 Range Error Influence

In CB, although the target's DOA is the only important parameter, the range is estimated to obtain the target's position more accurately in our design. We considered the perfect estimation of the target's range for equal comparison between our architecture and CB. The assumption of a perfect estimation is carried out by setting $d = \hat{d}$ in (3.26), where \hat{d} denotes the estimated distance from the reference sensor to the target and d signifies the target's true range. Estimating the target's range can increase the

level of accuracy of a target to a specific location instead of a particular direction.

In order to check the influence of the target's range estimation error, we further investigated the change in the beamformer response given in (3.26) when $d \neq \hat{d}$.

We have simulated the proposed beamformer beampattern with different range errors as a function of θ in Figure 3.6. It can be seen that the range estimation error can change beamformer performance by way of shifting the mainlobe direction and different attenuation on both sides of the mainlobe. As opposed to the range error influence in the frequency domain [22], the time-domain implementation is significantly less sensitive regarding the range error. This robustness can be seen in the way that the range estimation error negligibly affects the mainlobe position in the time domain. In contrast, small changes in the frequency domain can shift the position of the mainlobe by tens of degrees. In [22], this estimation error was addressed by adding another feedback beamformer. The minor effect of the estimation error in the time domain eliminates the use of an additional beamformer, which results in less hardware and a smaller footprint, which are critical considerations.

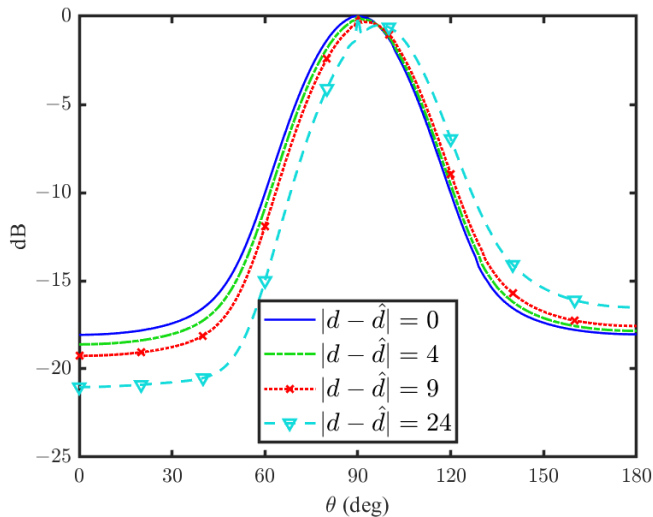


Figure 3.6 Effect of incorrect target range estimation for $\theta_d = 90^\circ$, $r = 0.6$, $N = 10$ and $\delta = 1\text{cm}$.

3.3.5 Summary

Chapter Summary

This chapter presented a detailed evaluation of the proposed feedback beamforming architecture, focusing on both its limitations and performance benefits. The discussion began with an investigation of channel gain estimation errors, which are inevitable in practical scenarios. It was shown that such inaccuracies can distort the beamformer response.

Subsequently, the proposed approach was compared to conventional beamformers that do not employ feedback. The results demonstrated that the feedback mechanism enhances spatial filtering capabilities by producing a narrower mainlobe and stronger sidelobe suppression. These improvements effectively increase the aperture of the system, yielding higher angular resolution and improved interference rejection, which are critical in many array processing applications.

The performance was further assessed through the analysis of the directivity factor, a key metric in beamforming evaluation. The findings confirmed that the suggested architecture provides a significant gain in directivity relative to traditional methods, thereby validating its ability to concentrate energy in the desired direction and generate higher directivity using much fewer elements.

Beyond the specific evaluations of error sensitivity, beamwidth, sidelobe attenuation, and directivity, this chapter highlights the broader potential of feedback-based beamforming as a design paradigm. The results underscore that incorporating recursive spatial responses can fundamentally extend the capabilities of conventional architectures, enabling sharper resolution and more resilient performance under practical uncertainties. This positions the feedback approach not only as a promising alternative, but also as a foundation for future advancements in robust real-time and high-performance array processing.

3.4 Time-Domain vs. Frequency-Domain Feedback Beamforming

In order to thoroughly investigate the proposed filter, we compared the proposed beamformer and the frequency-domain beamformer [22]. Some of the standard comparison measures include beamformer fidelity, the system's robustness, and computational complexity [34]. A comparison was made between time-frequency domain implementations according to the following additional parameters: the number of sensors used for the desired output, SNR, sampling frequency, data storage, processing requirements, and area considerations for implementing the hardware.

3.4.1 Calculation Complexity

Time-domain spatial filters offer distinct advantages over their frequency-domain counterparts, notably in computational efficiency. A significant benefit of time-domain processing, as demonstrated in the filter design outlined above (3.26), is its lower computational complexity relative to an analogous design in the frequency domain. Specifically, the most computationally intensive operation in the time-domain design is given by

$$\mathbf{G}^T(\hat{\theta}_d, \hat{d}) \left[\mathbf{G}(\hat{\theta}_d, \hat{d}) \mathbf{G}^T(\hat{\theta}_d, \hat{d}) \right]^{-1} \mathbf{G}(\theta_d, d).$$

This operation underscores the efficiency of time-domain designs in handling spatial filtering tasks. The focus is on minimizing the processing load without compromising the accuracy or effectiveness of the filtering process.

The above matrix multiplications require approximately $3N^2L_h^3$ multiplications and the same number of additions, where $N \gg 1$ and $L \approx L_h$. In the frequency-domain design, as defined and developed in [22], the beamformer is

$$\begin{aligned} H &= \frac{g\boldsymbol{\beta}^H \mathbf{d}e^{-j\phi}}{1 - g\boldsymbol{\alpha}^H \mathbf{d}e^{-j\phi}} \\ &= \left[1 - g \frac{e^{j\hat{\phi}} \hat{\mathbf{d}}^H}{\hat{g} \|\hat{\mathbf{d}}\|^2} \mathbf{d}e^{-j\phi} \right]^{-1} g \frac{e^{j\hat{\phi}} \hat{\mathbf{d}}^H}{\hat{g} \|\hat{\mathbf{d}}\|^2} \mathbf{d}e^{-j\phi} \end{aligned} \quad (3.29)$$

where \mathbf{d} is the steering vector, for which the n -th element is $d_n = \exp(-j\omega\tau_n)$, and ϕ is the round-trip signal propagation phase. One must consider the transform of each sensor signal to the frequency domain using the fast Fourier transform (FFT) and then use inverse FFT. Each time frame contains L_h samples, so each sensor requires $L_h \log_2 L_h$ operations. The FFT requires $NL_h \log_2 L_h$ operations. The most expensive operation in the filter design (3.29) is the multiplication of the steering vector by itself, which requires $4NL_h$ multiplications and the same number of additions, where the factor of 4 is due to the frequency-domain design dealing with complex numbers. The frequency-domain design requires approximately $4N^2L_h^2 \log_2 L_h$ multiplications and a similar number of additions. This shows that for sufficiently large NL_h , the frequency-domain beamformer incurs lower computational costs. Certain applications do not prioritize the beamformer's output signal in the time domain, so utilizing the frequency-domain beamformer would be more efficient. The above frequency-domain's complexity calculation assumes that L_h is an integer power of two. Otherwise, due to the FFT algorithm, zero padding must be added to each frame, which increases the computational complexity even more.

3.4.2 Execution Time

RADAR processing systems are based on pulse signals rather than continuous-wave (CW) stimuli. Although CW signals simplify system analysis, they are hardly feasible to implement and waste a significant part of the system's power; therefore, they are rarely used. Moreover, CW RADAR systems rarely measure distance, which is our primary goal. One main drawback when using pulse-based signals is the known fact that pulse signals, which are finite in the time domain, contain high frequencies. A practical pulse signal contains many more frequencies than a CW signal, which includes, in theory, only one frequency. Each of the frequencies is considered in the steering vector in the frequency domain, increasing the execution time of such a beamformer. Figure 3.7 demonstrates the differences in the time domain and in the power spectrum between CW and a pulse signal. As seen in the figures, the frequencies that must be

considered are orders of magnitude larger in the pulse-based signals than in the sine wave signals. Although just the sine frequency is a reasonable power in a sine wave, for the pulse-based signal, the power remains quite similar with increasing frequency.

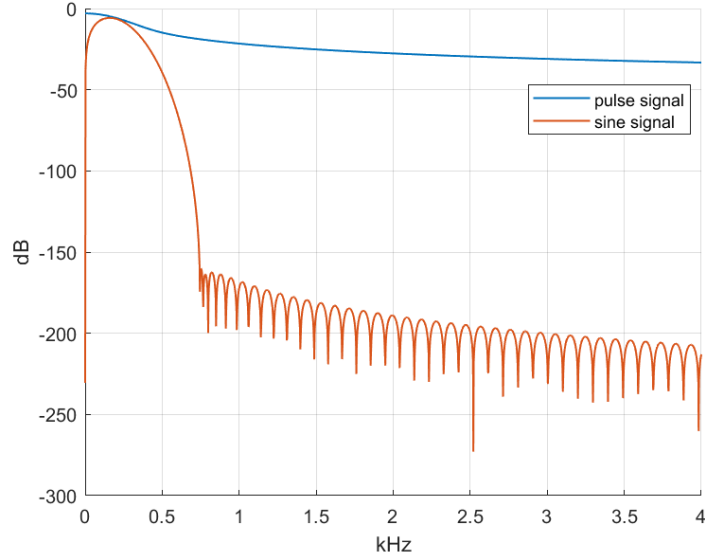


Figure 3.7 Power spectrum of both the pulse wave (blue line) and sine wave (red line) at the same sampling frequency.

This fact directly results from the execution time of the frequency-domain beamformer implementation. In [22], the beamformer computational complexity remains the same with the number of sensors. In order to authenticate this claim, in Figure 3.8, we show the execution time of the feedback beamformer in both the time and frequency domains as a function of the array size, where 10K frequencies are considered. This value is not a strict threshold, but rather a representative operating point reflecting the substantial spectral support of pulse-based signals, as evidenced by Figure 3.7. As can be seen from Figure 3.8, for a low number of sensors (up to 10 sensors), the time domain has a better execution time. In addition, one can see that the frequency-domain calculation time is on the scale of seconds, which is not feasible in real-time systems. The exponential increase in calculation time in the time domain is due to the growth of (3.12), and the samples must be taken at each interval.

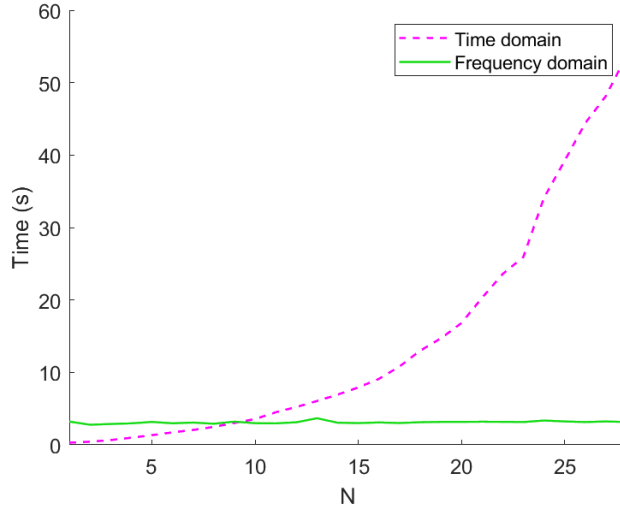


Figure 3.8 Execution time of the beamformer output for both time and frequency domains for $r = 0.6$, $\delta = 1cm$, when 10K frequencies are considered.

3.4.3 Summary

In this chapter, we summarize the main characteristics and trade-offs between time-domain and frequency-domain beamforming implementations. Table 3.1 highlights differences in computational complexity, latency, sensitivity to range errors, and hardware requirements, providing a concise comparison of the practical advantages and limitations of each approach.

Table 3.1 Comparison between Time-Domain and Frequency-Domain Beamforming Implementations

	Time-Domain	Frequency-Domain
Complexity	Direct operation on incoming signal; computational cost increases with number of sensors.	For sufficiently large NL_h , frequency-domain implementation incurs lower computational cost.
Latency	Low latency for small number of sensors (on the order of ms); increases exponentially with large arrays.	Higher latency due to block-based processing and Fourier transforms (on the order of seconds); weak dependence on the array's size in the measured range.
Sensitivity to range error	Minor effect on estimation error; mainlobe remains stable.	Significant displacement of the mainlobe can occur, making the system sensitive to range errors.
Hardware footprint	Smaller footprint; single architecture can handle range errors efficiently.	Requires doubled architecture to compensate for sensitivity to range errors, increased hardware requirements.

Chapter 4

Conclusions

This work has presented a closed-form formulation for a time-domain feedback-based beamformer, establishing a solid foundation for its theoretical development and practical application. The proposed feedback architecture demonstrated clear advantages over conventional methods, such as delay-and-sum and maximum directivity beamformers, while also confirming its equivalence to frequency-domain formulations. In doing so, the study bridges time and frequency-domain perspectives and broadens the design space for feedback beamforming.

Our analysis has shown that the time-domain realization offers superior robustness to range estimation errors compared with its frequency-domain counterpart. Moreover, the comparison of computational complexity and execution time revealed that implementation choice depends strongly on the number of sensors and data volume. Markedly, the time-domain beamformer achieves faster execution in settings with a limited number of sensors and pulse-based signaling, which are common in RADAR systems and critical for real-time use.

Overall, this work highlights both the theoretical contributions and the practical relevance of the proposed feedback beamforming framework. By combining analytical insight, robustness assessment, and complexity benchmarks, the study lays the groundwork for future extensions and applications in RADAR, communications, and sensing, pointing toward a new generation of high-performance, real-time beamforming architectures.

In the following, we outline several promising directions for future investigation of the FB concept.

4.1 Future Research

Having established the framework for the feedback-based beamforming architecture, the next chapter highlights several promising directions for future research. As mentioned in Sec. 3.1, We consider an idealized noiseless scenario, with a single stationary target in which the signals received by the beamformer elements consist exclusively of

the target’s impinging wavefront. A first direction for future research involves extending the analysis to noisy environments, where the received signals include both the target wavefront and noise components, thereby requiring explicit consideration of the SNR. Demonstrating the proposed architecture under such realistic RADAR conditions including pulsed RADAR target detection and range-Doppler profiling scenarios, represents a natural and high-priority direction for future experimental validation, through which the practical advantages of the proposed approach could be more concretely assessed and demonstrated. Another area of interest involves extending the current findings to scenarios involving nonstationary or multiple targets, enhancing the robustness of the beamformer in tracking moving targets within dynamic environments. As presented in Sec.3.2, the optimal beamformer weight coefficients were determined using the FIM, by accounting for both the contribution of the feedback mechanism and its supplementary information. A particularly promising avenue involves refining the design of feedback beamforming to enhance adaptive beamforming techniques. This includes dynamically adjusting the α and β coefficients within iterative processes to achieve improved performance compared to the static beamforming approach detailed in this research.

4.1.1 Noisy Environment

While the current research has been conducted under the assumption of an ideal noiseless environment, where the sampled signals consist solely of the impinging wave from the target, an important future direction is to extend the analysis to more realistic noisy conditions. In such settings, the received signal at each array element can be expressed as the sum of the desired target contribution and an additive noise component, thereby necessitating explicit consideration of the SNR. Investigating the feedback-based beamforming architecture under these conditions would provide valuable insights into its robustness and practical applicability, as well as establish performance limits when noise and interference are present.

4.1.2 Moving Target in Dynamic Environment

Revisiting (3.13), the proposed feedback beamforming framework, which has thus far been developed for static targets. An important direction for future research lies in extending this framework, to scenarios involving moving targets. In practical settings, such as RADAR, sonar, and wireless communications, targets are rarely stationary, and their motion introduces time-varying effects including Doppler shifts and dynamic delays. Addressing these challenges requires adaptive formulations capable of tracking motion while maintaining beamformer performance. Understanding how our method performs for static scenarios will be crucial for its practical deployment.

4.1.3 Multi Target

Another promising avenue for future research is the extension of the feedback beamforming framework to scenarios involving multiple simultaneous targets. In real-world environments, sensor arrays are often required to process signals originating from several sources of interest while simultaneously suppressing interference and noise. The presence of multiple targets introduces additional challenges, such as increased spatial correlation, overlapping wavefronts, and the need to resolve signals arriving from closely spaced directions.

Promising avenues for future research include:

- Analyzing the maximum number of simultaneously resolvable targets as a function of the array size N .
- Examining the achievable localization resolution under varying conditions.

4.1.4 Adaptive Feedback Beamforming

Another promising direction for future research is the development of adaptive feedback-based beamforming. As outlined previously, a key factor in determining beamformer performance lies in the selection of the optimal weight coefficients. In the present study, the analysis was restricted to a fixed beamformer, where both the feedback and output filter coefficients remain constant. However, a complementary study should explore adaptive strategies, in which these coefficients evolve dynamically over time to adjust to the characteristics of the received signals and the environment. Such an approach has the potential to significantly enhance the robustness and flexibility of the feedback beamforming architecture, particularly in non-stationary or rapidly changing scenarios.

Appendix A

Fisher Information Matrix

In parameter estimation problems, the objective is to infer unknown parameters from a sample of data drawn from an underlying probability distribution. The Fisher Information Matrix provides a fundamental tool to quantify the amount of information contained in the data with respect to the parameters of interest.

Let X be a random variable with probability density function (PDF) $f(x|\theta)$, where $\theta \in \Theta$ is the unknown parameter. Intuitively, the occurrence of a low-probability event provides more information about the true parameter value. If θ were indeed the true parameter, the likelihood function would attain a relatively large value. Equivalently, the derivative of the log-likelihood function would approach zero, forming the basis of ML estimation. Defining the log-likelihood as

$$l(x|\theta) = \log f(x|\theta),$$

the Fisher information matrix is expressed [32] as

$$\mathbf{I}(\theta) = -\mathbb{E}_\theta \left\{ \frac{\partial^2}{\partial \theta^2} \log f(x|\theta) \right\} = - \int \left[\frac{\partial^2}{\partial \theta^2} \log f(x|\theta) f(x|\theta) \right] dx.$$

A.0.1 Cramér–Rao Lower Bound

In practical applications where noise is present, parameters cannot generally be estimated with arbitrary precision. The FIM naturally leads to the *CRLB*, which establishes a lower bound on the variance of any unbiased estimator. Specifically, for an unbiased estimator $\hat{\theta}$, we have [32]

$$\text{Var}_\theta\{\hat{\theta}\} \geq \mathbf{I}^{-1}(\theta).$$

This bound demonstrates that no unbiased estimator can achieve a variance below the CRLB. Thus, the CRLB provides a benchmark for evaluating the efficiency of estimators.

A.0.2 Multiple-Parameter Case

For models with multiple unknown parameters, let $\boldsymbol{\theta} = (\theta_0, \dots, \theta_{k-1})^T$, and let $X \sim f(x|\boldsymbol{\theta})$. The log-likelihood function is

$$l(\boldsymbol{\theta}) = \log f(x|\boldsymbol{\theta}),$$

with gradient (score vector)

$$\frac{\partial l(\boldsymbol{\theta})}{\partial \boldsymbol{\theta}} = \left(\frac{\partial l(\boldsymbol{\theta})}{\partial \theta_0}, \dots, \frac{\partial l(\boldsymbol{\theta})}{\partial \theta_{k-1}} \right)^T.$$

The Hessian matrix of second derivatives is

$$\frac{\partial^2 l(\boldsymbol{\theta})}{\partial \boldsymbol{\theta}^2} = \left\{ \frac{\partial^2 l(\boldsymbol{\theta})}{\partial \theta_i \partial \theta_j} \right\}_{i,j \in [0, \dots, k-1]}.$$

The Fisher Information Matrix is then defined as

$$\mathbf{I}(\boldsymbol{\theta}) = \mathbb{E} \left\{ \frac{\partial l(\boldsymbol{\theta})}{\partial \boldsymbol{\theta}} \left(\frac{\partial l(\boldsymbol{\theta})}{\partial \boldsymbol{\theta}} \right)^T \right\} = \text{Cov} \left\{ \frac{\partial l(\boldsymbol{\theta})}{\partial \boldsymbol{\theta}} \right\} = -\mathbb{E} \left\{ \frac{\partial^2 l(\boldsymbol{\theta})}{\partial \boldsymbol{\theta}^2} \right\}.$$

Since the covariance matrix is symmetric and positive semi-definite, the Fisher Information Matrix inherits these properties.

A.0.3 Applications of the FIM

For unbiased estimators in the multi-parameter setting, the CRLB generalizes to

$$\text{Cov}_{\boldsymbol{\theta}}\{\hat{\boldsymbol{\theta}}(X)\} \geq \mathbf{I}^{-1}(\boldsymbol{\theta}),$$

where the inequality is interpreted in the sense of positive semi-definiteness. From this expression, it follows that a larger determinant of $\mathbf{I}(\boldsymbol{\theta})$ implies a smaller CRLB, indicating that the data contains more information. Although the bound may not always be achievable in practice, it serves as a theoretical benchmark for the accuracy of parameter estimators.

Appendix B

FIM Calculation

A full proof of the FIM main diagonal elements is presented, yielding (3.23). By combining (3.19) and $z[m] = \boldsymbol{\beta}^T \mathbf{x}[m]$, we calculate the partial derivatives, $\frac{\partial z[m]}{\partial \theta_d}$ and $\frac{\partial z[m]}{\partial d}$:

$$\begin{aligned} \frac{\partial z[m]}{\partial \theta_d} &= \frac{\partial}{\partial \theta_d} \frac{g_c \boldsymbol{\beta}^T \mathbf{G}(\theta_d, d) \mathbf{s}[m]}{1 - g_c \boldsymbol{\alpha}^T \mathbf{G}(\theta_d, d) \mathbf{i}_\ell} \\ &= \frac{g_c \boldsymbol{\beta}^T \frac{\partial}{\partial \theta_d} \mathbf{G}(\theta_d, d) \mathbf{s}[m] \left[1 - g_c \boldsymbol{\alpha}^T \mathbf{G}(\theta_d, d) \mathbf{i}_\ell \right]}{\left[1 - g_c \boldsymbol{\alpha}^T \mathbf{G}(\theta_d, d) \mathbf{i}_\ell \right]^2} \\ &\quad + \frac{g_c \boldsymbol{\alpha}^T \frac{\partial}{\partial \theta_d} \mathbf{G}(\theta_d, d) \mathbf{i}_\ell g_c \boldsymbol{\beta}^T \mathbf{G}(\theta_d, d) \mathbf{s}[m]}{\left[1 - g_c \boldsymbol{\alpha}^T \mathbf{G}(\theta_d, d) \mathbf{i}_\ell \right]^2} \end{aligned} \quad (\text{B.1})$$

and

$$\begin{aligned} \frac{\partial z[m]}{\partial d} &= \frac{\partial}{\partial d} \frac{g_c \boldsymbol{\beta}^T \mathbf{G}(\theta_d, d) \mathbf{s}[m]}{1 - g_c \boldsymbol{\alpha}^T \mathbf{G}(\theta_d, d) \mathbf{i}_\ell} \\ &= \frac{g_c \boldsymbol{\beta}^T \frac{\partial}{\partial d} \mathbf{G}(\theta_d, d) \mathbf{s}[m] \left[1 - g_c \boldsymbol{\alpha}^T \mathbf{G}(\theta_d, d) \mathbf{i}_\ell \right]}{\left[1 - g_c \boldsymbol{\alpha}^T \mathbf{G}(\theta_d, d) \mathbf{i}_\ell \right]^2} \\ &\quad + \frac{g_c \boldsymbol{\alpha}^T \frac{\partial}{\partial d} \mathbf{G}(\theta_d, d) \mathbf{i}_\ell g_c \boldsymbol{\beta}^T \mathbf{G}(\theta_d, d) \mathbf{s}[m]}{\left[1 - g_c \boldsymbol{\alpha}^T \mathbf{G}(\theta_d, d) \mathbf{i}_\ell \right]^2}. \end{aligned} \quad (\text{B.2})$$

Recall that a derivative, which is a matrix with a scalar, is a derivative of each element, and the partial derivatives of $\mathbf{G}_{n_{ij}}$ can be written as

$$\frac{\partial \mathbf{G}_{n_{ij}}}{\partial \theta_d} = \frac{\partial}{\partial \theta_d} \text{sinc} \left(-P - i + j - \Delta - \frac{f_s n \delta \cos(\theta_d)}{c} \right). \quad (\text{B.3})$$

By defining $A = -P - i + j$, $B = \Delta$ and $D = \frac{f_s n \delta}{c}$, we obtain

$$\begin{aligned} \frac{\partial}{\partial \theta_d} \text{sinc}(A - B - D \cos(\theta_d)) &= \frac{\pi D \cos[\pi(A - B - D \cos(\theta_d))] \sin(\theta_d) [A - B - D \cos(\theta_d)]}{\pi [A - B - D \cos(\theta_d)]^2} \\ &\quad - \frac{D \sin(\theta_d) \sin[\pi(A - B - D \cos(\theta_d))]}{\pi [A - B - D \cos(\theta_d)]^2}. \end{aligned} \quad (\text{B.4})$$

By denoting $F = A - B - D \cos(\theta_d)$, we have

$$\frac{\partial}{\partial \theta_d} \text{sinc}(A - B - D \cos(\theta_d)) = \frac{\pi D \cos(\pi F) \sin(\theta_d) F - D \sin(\theta_d) \sin(\pi F)}{\pi F^2}. \quad (\text{B.5})$$

Since δ is at the scale of centimeters (at most) for a common ULA architecture, and assuming typical sample rates (f_s) of ULA usage, we obtain $D \ll 1$, $B \ll 1$, and $F \in \mathbb{Z}$. In accordance with trigonometric identities, we can conclude that $\cos(\pi F) = -1$ and $\sin(\pi F) = 0$. In conclusion, the partial derivative, with respect to θ_d , is given by

$$\frac{\partial \mathbf{G}_{n_{ij}}}{\partial \theta_d} = -\frac{\pi D \sin(\theta_d) F}{\pi F^2} = -\frac{D \sin(\theta_d)}{F}. \quad (\text{B.6})$$

In the same way as for $\frac{\partial \mathbf{G}_{n_{ij}}}{\partial d}$, recall that for $\Delta = f_s \tau_{pd} = f_s \frac{2d}{c}$, we obtain $A = -P - i + j$, $B = f_s \frac{2}{c}$ and $C = f_s \tau_n$ such that

$$\begin{aligned} \frac{\partial \mathbf{G}_{n_{ij}}}{\partial d} &= \frac{\partial}{\partial d} \text{sinc}(A - Bd - C) = \\ &\quad - \frac{\pi B \cos[\pi(A - Bd - C)] (A - Bd - C)}{\pi [A - Bd - C]^2} \\ &\quad + \frac{B \sin[\pi(A - Bd - C)]}{\pi [A - Bd - C]^2}. \end{aligned} \quad (\text{B.7})$$

By denoting $F = A - Bd - C$, we have

$$\frac{\partial \mathbf{G}_{n_{ij}}}{\partial d} = B \frac{-\pi \cos(\pi F) F + \sin(\pi F)}{\pi F^2}. \quad (\text{B.8})$$

Similar to before, $C \ll 1$. Additionally, $f_s \ll c$; therefore, $B \ll 1$ and $F \in \mathbb{Z}$. Thus, $\cos(\pi F) = -1$ and $\sin(\pi F) = 0$. In conclusion, the partial derivative with respect to d is given by

$$\frac{\partial \mathbf{G}_{n_{ij}}}{\partial d} = \frac{\pi B F}{\pi F^2} = \frac{B}{F}. \quad (\text{B.9})$$

By substituting (B.6) and (B.9) into (B.1) and (B.2), correspondingly, and performing further partial derivatives, we obtain f_1 and f_2 , respectively.

Bibliography

- [1] Z. Geng, H. Deng, and B. Himed, “Adaptive Radar Beamforming for Interference Mitigation in Radar-wireless Spectrum Sharing,” *IEEE Signal Processing Letters*, vol. 22, no. 4, pp. 484–488, 2014.
- [2] A. E. A. Blomberg, A. Austeng, R. E. Hansen, and S. A. V. Synnes, “Improving Sonar Performance in Shallow Water using Adaptive Beamforming,” *IEEE Journal of Oceanic Engineering*, vol. 38, no. 2, pp. 297–307, 2013.
- [3] G. E. Allen and B. L. Evans, “Real-time Sonar Beamforming on Workstations using Process Networks and POSIX Threads,” *IEEE Transactions on Signal Processing*, vol. 48, no. 3, pp. 921–926, 2000.
- [4] Z. Lin, M. Lin, J.-B. Wang, Y. Huang, and W.-P. Zhu, “Robust Secure Beamforming for 5g Cellular Networks Coexisting with Satellite Networks,” *IEEE Journal on Selected Areas in Communications*, vol. 36, no. 4, pp. 932–945, 2018.
- [5] A. H. Phan, H. D. Tuan, and H. H. Kha, “Space-time Beamforming for Multiuser Wireless Relay Networks,” *IEEE International Conference on Acoustics, Speech and Signal Processing (ICASSP)*, pp. 2836–2839, 2011.
- [6] A. J. Paulraj and C. B. Papadias, “Space-time Processing for Wireless Communications,” *IEEE Signal Processing Magazine*, vol. 14, no. 6, pp. 49–83, 1997.
- [7] Z. Lin, H. Niu, K. An, Y. Wang, G. Zheng, S. Chatzinotas, and Y. Hu, “Refracting RIS-aided Hybrid Satellite-terrestrial Relay Networks: Joint Beamforming Design and Optimization,” *IEEE Transactions on Aerospace and Electronic Systems*, vol. 58, no. 4, pp. 3717–3724, 2022.
- [8] K. An, M. Lin, J. Ouyang, and W.-P. Zhu, “Secure Transmission in Cognitive Satellite Terrestrial Networks,” *IEEE Journal on Selected Areas in Communications*, vol. 34, no. 11, pp. 3025–3037, 2016.
- [9] K. Schuler, M. Younis, R. Lenz, and W. Wiesbeck, “Array Design for Automotive Digital Beamforming Radar System,” *IEEE International Radar Conference*, pp. 435–440, 2005.

- [10] M. Harter, J. Hildebrandt, A. Zioff, and T. Zwick, “Self-calibration of a 3-D-digital Beamforming Radar System for Automotive Applications with Installation behind Automotive Covers,” *IEEE Transactions on Microwave Theory and Techniques*, vol. 64, no. 9, pp. 2994–3000, 2016.
- [11] E. J. Bond, X. Li, S. C. Hagness, and B. D. Van Veen, “Microwave Imaging via Space-time Beamforming for Early Detection of Breast Cancer,” *IEEE Transactions on Antennas and Propagation*, vol. 51, no. 8, pp. 1690–1705, 2003.
- [12] D. Byrne and I. J. Craddock, “Time-domain Wideband Adaptive Beamforming for Radar Breast Imaging,” *IEEE Transactions on Antennas and Propagation*, vol. 63, no. 4, pp. 1725–1735, 2015.
- [13] Z. Lin, H. Niu, K. An, Y. Hu, D. Li, J. Wang, and N. Al-Dhahir, “Pain Without Gain: Destructive Beamforming from a Malicious RIS Perspective in IoT Networks,” *IEEE Internet of Things Journal*, vol. 11, no. 5, pp. 7619–7629, 2024.
- [14] Y. Sun, K. An, Y. Zhu, G. Zheng, K.-K. Wong, S. Chatzinotas, D. W. K. Ng, and D. Guan, “Energy-efficient Hybrid Beamforming for Multilayer RIS-assisted Secure Integrated Terrestrial-aerial Networks,” *IEEE Transactions on Communications*, vol. 70, no. 6, pp. 4189–4210, 2022.
- [15] J. Chen, K. Yao, and R. Hudson, “Source Localization and Beamforming,” *IEEE Signal Processing Magazine*, vol. 19, no. 2, pp. 30–39, 2002.
- [16] R. Schmidt, “Multiple Emitter Location and Signal Parameter Estimation,” *IEEE Transactions on Antennas and Propagation*, vol. 34, no. 3, pp. 276–280, 1986.
- [17] R. Roy and T. Kailath, “ESPRIT-Estimation of Signal Parameters via Rotational Invariance Techniques,” *IEEE Transactions on Acoustics, Speech, and Signal Processing*, vol. 37, no. 7, pp. 984–995, 1989.
- [18] Y. Chan and K. Ho, “A Simple and Efficient Estimator for Hyperbolic Location,” *IEEE Transactions on Signal Processing*, vol. 42, no. 8, pp. 1905–1915, 1994.
- [19] H. Krim and M. Viberg, “Two Decades of Array Signal Processing Research: The Parametric Approach,” *IEEE Signal Processing Magazine*, vol. 13, no. 4, pp. 67–94, 1996.
- [20] B. D. Van Veen and K. M. Buckley, “Beamforming: A Versatile Approach to Spatial Filtering,” *IEEE ASSP Magazine*, vol. 5, no. 2, pp. 4–24, 1988.
- [21] T. Chernyakova and Y. C. Eldar, “Fourier-domain Beamforming: The Path to Compressed Ultrasound Imaging,” *IEEE Transactions on Ultrasonics, Ferroelectrics, and Frequency Control*, vol. 61, no. 8, pp. 1252–1267, 2014.
- [22] I. Y. Karo, T. G. Dvorkind, and I. Cohen, “Source Localization with Feedback Beamforming,” *IEEE Transactions on Signal Processing*, vol. 69, pp. 631–640, 2020.

- [23] R. Dougherty, “Advanced Time-domain Beamforming Techniques,” *10th AIAA/CEAS Aeroacoustics Conference*, p. 2955, 2004.
- [24] Y. Buchris, I. Cohen, and J. Benesty, “On the Design of Time-domain Differential Microphone Arrays,” *Applied Acoustics*, vol. 148, pp. 212–222, 2019.
- [25] R. M. Shubair and A. Hakam, “Adaptive Beamforming using Variable Step-size LMS Algorithm with Novel ULA Array Configuration,” *2013 15th IEEE International Conference on Communication Technology*, pp. 650–654, 2013.
- [26] Z. Ye, J. Dai, X. Xu, and X. Wu, “DOA Estimation for Uniform Linear Array with Mutual Coupling,” *IEEE Transactions on Aerospace and Electronic Systems*, vol. 45, no. 1, pp. 280–288, 2009.
- [27] B. Liao and S.-C. Chan, “Adaptive Beamforming for Uniform Linear Arrays with Unknown Mutual Coupling,” *IEEE Antennas and Wireless Propagation Letters*, vol. 11, pp. 464–467, 2012.
- [28] C. E. Shannon, “Communication in the Presence of Noise,” *Proceedings of the IRE*, vol. 37, no. 1, pp. 10–21, 1949.
- [29] H. L. Van Trees, *Optimum Array Processing: Part IV of Detection, Estimation, and Modulation Theory*. John Wiley & Sons, 2002.
- [30] C. A. Balanis, *Antenna Theory: Analysis and Design*. John Wiley & Sons, 2016.
- [31] J. Benesty, I. Cohen, and J. Chen, *Fundamentals of Signal Enhancement and Array Signal Processing*. John Wiley & Sons, 2017.
- [32] A. Zeira and A. Nehorai, “Frequency Domain Cramer-Rao Bound for Gaussian Processes,” *IEEE Transactions on Acoustics, Speech, and Signal Processing*, vol. 38, no. 6, pp. 1063–1066, 1990.
- [33] S. V. Hum, *Radio and Microwave Wireless Systems*, <https://www.waves.utoronto.ca/prof/svhum/ece422/notes/15-arrays2.pdf>.
- [34] C. Bao, “Performance of Time Domain and Time-frequency Domain Adaptive Beamformers with Moving Sound Sources,” *INTER-NOISE and NOISE-CON Congress and Conference Proceedings*, vol. 249, no. 4, pp. 3727–3734, 2014.

באופן ישיר בין מבנה הרקורסיה לבין שיפור גבולות הביצוע התיאורטיים.

הארכיטקטורה המוצעת מוערכת הן באמצעות ניתוח תיאורטי והן באמצעות מדדי ביצוע קלאסיים של עיצוב אלומות -- רוחב אלומה, יחס שיא לאונה צדדית (Peak-to-Sidelobe Ratio) ודירקטיביות המערך. התוצאות מצביעות על שיפור מובהק ביחס למערכי Delay-and-Sum ולמערכי מקסימום דירקטיביות בכל המדדים שנבחנו. בנוסף, נערכת השוואה שיטתית בין מימוש בתחום הזמן לבין מימוש בתחום התדר, תוך בחינת מורכבות חישובית, שיהוי ודרישות דגימה. נמצא כי עבור מערכים בגודל מעשי, הגישה בתחום הזמן משיגה שיהוי נמוך יותר ומתאימה יותר ליישומים בזמן אמת.

הניתוח המקיף המוצג בעבודה זו נועד להוות בסיס תיאורטי מוצק למימושים עתידיים של עיצוב אלומה עם משוב במערכות RADAR יישומיות, לרבות גילוי מטרות בפולסים, אמידת טווח וסינון מרחבי בזמן אמת, תוך שמירה על יעילות חישובית ומימוש סיבתי.

תקציר

עיבוד מרחבי באמצעות מערכי חיישנים מהווה נדבך מרכזי בתחום עיבוד האותות, ומשמש תשתית מתמטית והנדסית ליישומים כגון איכון מקורות, דיכוי הפרעות, סינון מרחבי ושיפור יחס אות לרעש. ניצול המגוון המרחבי של מערך חיישנים מאפשר להפיק מידע גאומטרי מן האותות הנקלטים, ובפרט לאמוד פרמטרים פיזיקליים של מקור הקרינה, כגון כיוון ההגעה (Direction) of (Arrival) והטווח. ביצועי המערכת תלויים באופן מהותי בקונפיגורציה הפיזית של המערך -- מספר האלמנטים, מיקומם הגאומטרי והמפתח הכולל -- אשר מכתיבים את הרזולוציה הזוויתית, הדירקטיביות, רגישות האמידה ויכולת ההפרדה בין מקורות סמוכים.

מבין טכניקות העיבוד המרחבי, עיצוב אלומה (Beamforming) מספק מנגנון מובנה לסלקטיביות זוויתית באמצעות עיצוב תגובת המערך כך שתודגש אנרגיה מכיוון רצוי ותדוכא תרומה מכיוונים בלתי רצויים. גישות קלאסיות, ובהן Delay-and-Sum ו-Response Distortionless Variance Minimum (MVDR), ניתנות למימוש כמערכות מרחביות מסוג תגובה סופית (Finite Impulse Response). במסגרת זו, משקלי המערך מיושמים כמבנה הזנה קדמית, ולפיכך ביצועי הרזולוציה ודיוק האמידה חסומים עקרונית על ידי המפתח הפיזי של המערך. כלומר, כל שיפור במסגרת ארכיטקטורת FIR מרחבית כפוף למגבלת האפרטורה הנתונה, ואינו מאפשר חריגה מסדר החופש המרחבי שמוכתב על ידי מספר החיישנים והגאומטריה שלהם. מגבלה יסודית זו מניעה חיפוש אחר מבנים אלטרנטיביים החורגים מפרדיגמת ההזנה הקדמית.

עיצוב אלומה עם משוב (Feedback) (Beamforming) מציע פרדיגמה מבנית שונה, המבוססת על הכנסת רקורסיה מרחבית לשרשרת העיבוד. מבנה זה יוצר התנהגות מרחבית אנלוגית למערכת תגובה אינסופית (Infinite Impulse Response) ובכך מאפשר הרחבה אפקטיבית של המפתח הווירטואלי של המערך ללא הגדלת מספר החיישנים בפועל. בעוד שמימושים רקורסיביים קודמים נותחו בעיקר בתחום התדר, הארכיטקטורה המוצעת בעבודה זו ממומשת ישירות בתחום הזמן. מימוש זה מאפשר עיבוד סיבתי, שליטה ישירה בדינמיקה של המשוב, והתאמה לדרישות חישוביות של מערכות זמן אמת.

עבודה זו מפתחת מסגרת קוהרנטית ומלאה מבוססת תורת האמידה לעיצוב אלומה עם משוב בתחום הזמן, עבור אזור עניין בתחום השדה הרחוק. במסגרת זו נאמדים במשותף כיוון ההגעה והטווח של מטרה מחזירה, תוך ניתוח מפורש של הקשר בין מקדם המשוב, פונקציית התמסורת המרחבית והדיוק האסימפטוטי של האמידה. רגישות הפרמטרים מאופיינת באמצעות מטריצת המידע של פישר (Fisher Information Matrix), ומתוכה נגזרים גבולות קרמר--ראו (Cramer-Rao Lower Bounds) עבור האמידה המשותפת. הניתוח מראה כי כאשר מקדם המשוב מתקרב לערכו האופטימלי, המכנה של פונקציית התמסורת המרחבית שואף לאפס, תופעה המובילה להגברת התגובה המרחבית ולהגדלת רגישות הפרמטרים. תוצאה זו מספקת פורמליזציה כמותית למושג הרחבת המפתח הווירטואלי, ומקשרת

המחקר בוצע בהנחייתו של פרופסור ישראל כהן, בפקולטה להנדסת חשמל ומחשבים.

חלק מן התוצאות בחיבור זה פורסמו כמאמרים מאת המחבר ושותפיו למחקר בכנסים ובכתבי-עת במהלך תקופת מחקר המגיסטר של המחבר, אשר גרסאותיהם העדכניות ביותר הינן:

Z. A. Herscovici and I. Cohen, "Feedback beamforming in the time domain," *Sensors*, vol. 24, no. 7, p. 2179, 2024.

מחבר חיבור זה מצהיר כי המחקר, כולל איסוף הנתונים, עיבודם והצגתם, התייחסות והשוואה למחקרים קודמים וכו', נעשה כולו בצורה ישרה, כמצופה ממחקר מדעי המבוצע לפי אמות המידה האתיות של העולם האקדמי. כמו כן, הדיווח על המחקר ותוצאותיו בחיבור זה נעשה בצורה ישרה ומלאה, לפי אותן אמות מידה.

תודות

ראשית, אני רוצה להודות מעומק הלב למנחה שלי, פרופ' ישראל כהן, על ההכוונה הבלתי תחליפית וההבנה הקריטית, וכן על כך ששיתף אותי נדיבות בידע ובניסיון הרחב שלו. ההכוונה והתמיכה שלו עשו את העבודה הזו אפשרית. אני אסיר תודה על ההזדמנויות שהוא העניק לי ועל האמון שהעניק לי לאורך הדרך.

בנוסף, אני רוצה להודות למשפחתי, להוריי ואחיותיי, ולבת זוגתי, ליאור, אשר יצרו סביבה תומכת ומכילה, שהאיצה את עבודתי ונתנה לי את הביטחון והיכולת לבצע אותה בצורה מיטבית. אני חב להם מאוד, שכן הישג זה לא היה מתממש ללא תרומתם.

אני מודה לטכניון על התמיכה הכספית הנדיבה בהשתלמותי.

עיצוב אלומה מבוסס משוב במישור הזמן

חיבור על מחקר

לשם מילוי חלקי של הדרישות לקבלת התואר
מגיסטר למדעים בהנדסת חשמל

צבי אהרן הרשקוביץ

הוגש לסנט הטכניון – מכון טכנולוגי לישראל
טבת התשפ"ו חיפה ינואר 2026

עיצוב אלומה מבוסס משוב במישור הזמן

צבי אהרן הרשקוביץ